学位論文

Study of chiral transport phenomena in a parallel electric and magnetic field

（平行な電場と磁場の下でのカイラル輸送現象の研究）

２０２２年３月

青井 隼斗

Abstract

The chiral anomaly is a phenomenon in which the conservation law for axial currents is violated by quantum effects. In recent years, when a magnetic field is applied to a system with chirality imbalance, the chiral anomaly generates vector current flow in the same direction as the magnetic field. This phenomenon is known as chiral magnetic effect (CME). Together with other similar effects, such anomaly induced transport processes are called the chiral transport phenomena and have been actively studied in a wide range of fields. In this thesis, in order to provide a theoretical basis for the chiral transport phenomena, we investigate the response of a vacuum and a system with a finite number of fermions to a spatial-homogeneous and static magnetic field and a parallel time-varying electric field as external fields. In particular, we investigate the generation of chirality imbalance and chiral transport phenomena and clarify the relationship with the chiral anomaly. We obtain exact solutions of the Dirac equation under the electromagnetic field and quantize the field using the canonical quantization method. In addition, we describe the particle production from vacuum by the Schwinger mechanism, which helps a microscopic understanding the chiral transport. By introducing Bogoliubov transformations, the expectation values of physical quantities are linked to the particle pair production by the electric field. As a result, we find that the chirality imbalance and CME current are generated by the electric field and strongly depend on the time dependence of the electric field. The role of the fermion mass is also systematically investigated. These results are important for the fundamental study of the chiral transport phenomena and provide a guideline for future applications.

CONTENTS

I. INTRODUCTION

Conservation laws are the most fundamental laws in physics. In classical field theories, a symmetry of the action is associated with a conservation law, as known Noether's theorem. Considering the action of a charged fermion field in a electromagnetic field, $S = \int d^4x[\bar{\psi}(i\partial_\mu - eA_\mu)\gamma^\mu\psi - m\bar{\psi}\psi]$, the conservation of vector current(charge conservation), $\partial_\mu\bar{\psi}\gamma^\mu\psi = 0$, is derived by the invariance of action under the global phase transformation of the fermion field, $\psi \to e^{i\alpha}\psi$.

In the relativistic field theory of fermion, chirality and chiral symmetry are essential concepts. Chirality is related to the sign of the projection of the fermion's spin onto its momentum. If a fermion's spin and momentum are (anti-)parallel, then the fermion is (left)right-handed. In the case of antifermions, if the spin and momentum are (anti-)parallel, then the fermion is (right)left-handed. The chiral transformation is a continuous transformation defined by $\psi \to \mathrm{e}^{i\alpha\gamma_5}\psi$. From the Noether's theorem, the chiral transformation is associated with the conservation law of the axial-vector current, $\partial_\mu\bar{\psi}\gamma^\mu\gamma^5\psi = 2m\bar{\psi}i\gamma^5\psi$. In particular, the 0th-component of axial-vector current, $\bar{\psi}\gamma^0\gamma^5\psi = \psi_R^\dagger\psi_R - \psi_L^\dagger\psi_L \equiv n_5$, is called *chirality imbalance*, which means the number difference between right- and left-handed fermions. If the fermion is massless, then the action of the fermion field has the chiral symmetry, and the axial-vector current is completely conserved even in the presence of an electromagnetic field.

However, in quantum field theory, the conservation law of the axial-vector current is violated. It is known as the chiral anomaly (Adler-Bell-Jackiw anomaly). The chiral anomaly adds a quantum correction term proportional to the inner product of the electric and magnetic fields. The chiral anomaly implies that chirality imbalance n_5 can be dynamically produced by an external electromagnetic field. This is a phenomenon unique to the quantum field theory.

In recent years, it has been suggested that the chiral anomaly may be observed as macroscopic transport phenomena. The most intriguing one is chiral magnetic effect(CME), which is the appearance of an electric current along the external magnetic field in the presence of chirality imbalance. The CME current is represented by CME formula, $\boldsymbol{j}^V = \frac{e^2}{2\pi^2}\mu_5\boldsymbol{B}$, where $\boldsymbol{j}^V$ is the electric current, and μ_5 is the chiral chemical

potential. The chiral chemical potential μ_5 represents an asymmetry of the chirality in the system and is conjugate to the chirality imbalance, n_5. It is expected that the CME current can be observed in heavy-ion collisions and Dirac/Weyl semimetals.

Another interesting anomalous transport phenomenon is the chiral separation effect (CSE), which is the generation of axial-vector current along the direction of the magnetic field. The CSE formula is represented by $\boldsymbol{j}^A = \frac{\mu}{2\pi^2}\boldsymbol{B}$, where μ is the fermion chemical potential and $\boldsymbol{j}^A$ is the space component of the axial-vector current interpreted as the expectation value of spin. The chiral separation effect has been discussed in a dense matter system under a strong magnetic field such as compact stars. The coupling between CME and CSE causes a gapless collective mode in the presence of an external magnetic field, referred to as chiral magnetic wave (CMW). So a comprehensive analysis that takes into account not only CME but also CSE is important.

From a theoretical view, however, the CME current in equilibrium systems needs to be handled with care since the introduction of the chiral chemical potential μ_5 in the equilibrium system is a subtle issue. It seems that the introduction of the chiral chemical potential implicitly assumes a system out of equilibrium. Moreover, in most of the previous works for the chiral transport, the introduction to chiral chemical potential μ_5 (or almost equivalently chirality imbalance n_5) is *a priori* assumption. However, the production process of the initial chirality imbalance is still in debate. In order to clarify this problem, it is crucial to explicitly calculate the time evolution of chirality imbalance within a specific model and compare their characteristic timescales.

In addition, the fermion mass dependence of the CME and CSE currents is also significant because the chirality imbalance strongly depends on the fermion mass. In the case of massless fermion, right- and left-handed fermions are separated in the equation of motions, but if the fermion has nonzero mass, the chiral symmetry is explicitly broken, and right- and left-handed fermions are mixed in their equations of motion. So it is important to investigate the production of the chirality imbalance for the massive fermion by a parallel electric and magnetic field.

In the strong parallel electric and magnetic field, it is known that the chiral anomaly is related to the pair production from the vacuum by the strong electric field, known as

Schwinger pair production. Schwinger computed the pair production rate per unit volume and time in a spatial-homogeneous static electric field, $w \sim \exp\left(-\frac{\pi m^2}{eE}\right)$, which m is the mass of the fermion and eE is the strength of the electric field. This formula implies that the vacuum becomes unstable above the critical electric field, $eE_c \sim m^2$, and the mass of fermions exponentially suppresses the production rate. Another point worth noting is that the formula is non-analytic in the coupling constant e, which indicates the nonperturbative nature of the Schwinger pair production.

In a parallel electric and magnetic field, the production rate of the chirality imbalance can be related to the Schwinger pair production rate. In the view of productions of chirality imbalance by an external electromagnetic field, it is expected that the asymmetry of momentum and spin caused by a parallel electric and magnetic field play important roles to understand the chiral anomaly. Since the Schwinger pair production is a nonperturbative phenomenon of the field theory, we need to use a nonperturbative method to investigate the chiral anomaly and the pair productions.

In this thesis, in order to provide a theoretical basis for chiral transport phenomena, we investigate the response of a system with a zero/finite number of fermions to a spatial-homogeneous and static magnetic field and a parallel time-varying electric field as external fields. In particular, we investigate the time-dependence of chirality imbalance and clarify the relationship with the chiral anomaly. We use the solution of the Dirac equation in the parallel electric and magnetic field without the chiral chemical potential. The field operator is expanded by the solution of the Dirac equation and the canonical quantization is performed, then the vacuum state and the finite Fermi energy system are constructed. Moreover, using the Bogoliubov transformation, we can obtain the time-dependent momentum distribution of pair produced particles described by Bogoliubov coefficients. The Bogoliubov transformation is helpful to understand the nonperturbative nature of chiral anomaly from microscopic views.

This thesis is based on our recent publications[1][2] and organized as follows. First, the background of the study is explained in Chapters 2 to 4. In Chapter 2, we describe the chiral anomaly and chirality imbalance, which are the theoretical basis of this study. In Chapter 3, we explain the theoretical background and the present status of experimental

observations of the chiral transport phenomenon and then present the problems of the theoretical formulation. In Chapter 4, we introduce the historical background of the Schwinger pair production and its connection with the chiral anomaly. In Chapters 5 to 7, we formulate methods used in this study. First, in Chapter 5, we derive the solution of the Dirac equation under a parallel electric and magnetic field. Then, in Chapter 6, the fermionic field operator expanded by the solution of the Dirac equation is quantized using the canonical quantization method to obtain the expectation value of the physical quantity. In Chapter 7, we introduce Bogoliubov transformations and describe the physical quantities obtained in Chapter 6 in terms of Bogoliubov variables that contain information on the Schwinger pair production. In Chapters 8 and 9, we present numerical results based on the formulation. In Chapter 8, the time evolution of physical quantities when the number of particles is zero is presented, focusing on the fermion mass. In Chapter 9, the same analysis as in Chapter 8 is performed for the case of a finite number of particles. Finally, in Chapter 10, the conclusion of this thesis is given.

II. CHIRAL ANOMALY

Conservation laws are the most fundamental laws in physics. From Noether's theorem, conservation laws are associated with symmetries in the theory. The term *symmetry* means the invariance of the action under the continuous transformation of a field. It is known that translational(rotational) symmetry of spacetime leads to the conservation law of energy-momentum (angular momentum). Considering the action of a charged fermion field in a electromagnetic field,

$$S = \int d^4x[\bar{\psi}(i\partial_\mu - eA_\mu)\gamma^\mu\psi - m\bar{\psi}\psi], \tag{1}$$

the invariance of the global phase transformation of the fermion field, $\psi \to e^{i\alpha}\psi$, is associated with the conservation law of the vector current, $\partial_\mu\bar{\psi}\gamma^\mu\psi = 0$. The gauge invariance is one of the most important guiding principles in quantum field theories because the conservation law of the vector current(or equivalently charge conservation) has been confirmed experimentally up to the present.

Chiral symmetry is ne of the most fundamental symmetries in relativistic quantum field theories, such as quantum electrodynamics(QED) and quantum chromodynamics(QCD), which is the invariance of actions under the continuous transformation, $\psi \to \mathrm{e}^{i\alpha\gamma_5}\psi$, called chiral transformation. Here γ^5 is the chirality operator defined by $\gamma^5 \equiv i\gamma^0\gamma^1\gamma^2\gamma^3$. Chirality is essential for massless fermions, which is related to the sign of the projection of the fermion's spin onto its momentum. If the eigenvalue of the chirality operator is positive, then the fermion is right-handed (its spin and momentum are parallel), and if it is negative, then the fermion is left-handed (its spin and momentum are anti-parallel). In the case of antifermions, if the eigenvalue is positive (negative), the antifermion is left(right)-handed. A Dirac spinor is projected onto the right(left)-handed spinor, $\psi_{R/L} \equiv P_{R/L}\psi$, by using the chirality projection operator, $P_{R/L} = \frac{1\pm\gamma^5}{2}$. In the case of massless fermions, the theory has chiral symmetry, and $\psi_{R/L}$ obeys independent equations of motion. If the fermion has nonzero mass, the chiral symmetry is explicitly broken, and $\psi_{R/L}$ are mixed in their equations of motion.

From the Noether's theorem, the chiral transformation is associated with the conser-

vation law of the axial-vector current,

$$\partial_\mu \bar{\psi}\gamma^\mu\gamma^5\psi = 2m\bar{\psi}i\gamma^5\psi \tag{2}$$

where m is the mass of fermions, and $\bar{\psi}i\gamma^5\psi$ is called pseudoscalar condensation. The conservation law is satisfied even if the fermion field is coupled to gauge fields. In the case of massless fermion, the axial-vector current is conserved.

However, sometimes a conservation law satisfied in the classical theory is violated by quantum effects. This phenomenon is called *anomaly*, and it is one of the essential topics in high-energy physics and condensed matter physics. The most famous example is the chiral anomaly. The chiral anomaly is found by Adler, Bell, and Jackiw[3][4], so often called the Adler-Bell-Jackiw anomaly. The chiral anomaly violates the conservation law for the vacuum expectation value of axial-vector current expressed as follows,

$$\int d^3x\partial_\mu\langle\bar{\psi}\gamma^\mu\gamma^5\psi\rangle = 2m\int d^3x\langle\bar{\psi}i\gamma^5\psi\rangle + \frac{2\alpha}{\pi}\int d^3x\boldsymbol{E}\cdot\boldsymbol{B} \tag{3}$$

with $\alpha = e^2/4\pi$ being the fine structure constant and the last term comes from quantum corrections. The relation (3) is called anomaly relation or axial Ward identity. It can be derived by some methods: calculating the axial-vector current operator equation in a background gauge field, triangle diagrams (shown in Fig.1) in standard perturbation theory, and functional integral for the fermion field. The anomaly relation is found not only in abelian gauge theories(such as QED) but also in non-abelian ones(such as QCD) and also valid at finite temperature and finite density[5].

The chiral anomaly causes the $\mathcal{CP}$-violating measurable processes. It is widely known that the chiral anomaly contributes to the matrix element for the decay of the neutral pion into two photons, $\pi_0 \to 2\gamma$. The neutral pion decays through a one-loop triangle diagram (as in Fig.1) into two photons, and the decay rate is tested experimentally to a high degree of accuracy. More recently, macroscopic transport phenomena due to anomalies have been studied, which will be discussed in detail in the next chapter.

It is well known that the conservation of the axial-vector current is incompatible with gauge invariance. If the conservation of axial-vector current due to chiral symmetry is respected, then the conservation of vector current due to gauge symmetry is violated, or vice versa. The nature of chiral anomaly is caused by the regularization of contributions

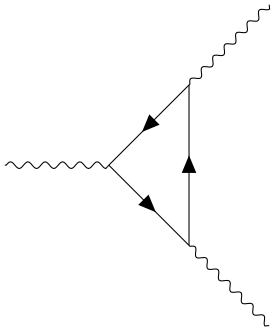

FIG. 1. A triangle diagram.

from the vacuum in which an infinite number of fermions(antifermions) are occupied. So we have to treat carefully the momentum integral in the expectation value of axial-vector current with noting the gauge-invariance.

The 0th-component of axial-vector current, $\langle\bar{\psi}\gamma^0\gamma^5\psi\rangle = \langle\psi_R^\dagger\psi_R - \psi_L^\dagger\psi_L\rangle \equiv n_5$, is called *chirality imbalance*, which means the number difference between right- and left-handed fermions. The anomaly relation (3) implies that an external electromagnetic field can produce chirality imbalance. The 1+1 massless fermi system in the Dirac sea picture helps intuitively understand the chirality imbalance production by the external field(Fig.2). In the 1+1 dimensional system, electric fields can exist, and magnetic fields do not exist. The dispersion relation of massless fermions is linear (Fig.2(a)), and gapless excitations can occur by an electric field. A hole created by a particle in a negative energy state being kicked out into a positive energy state behaves as an antiparticle(Fig.2(b)). In the 1+1 dimensional system, particles with positive energy and positive momentum are right-handed, and the corresponding holes are also right-handed so that chirality imbalance is produced after an electric field applied. In the later section, we will discuss the production of chirality imbalance by a parallel electric and magnetic field in a 1+3 dimensional system.

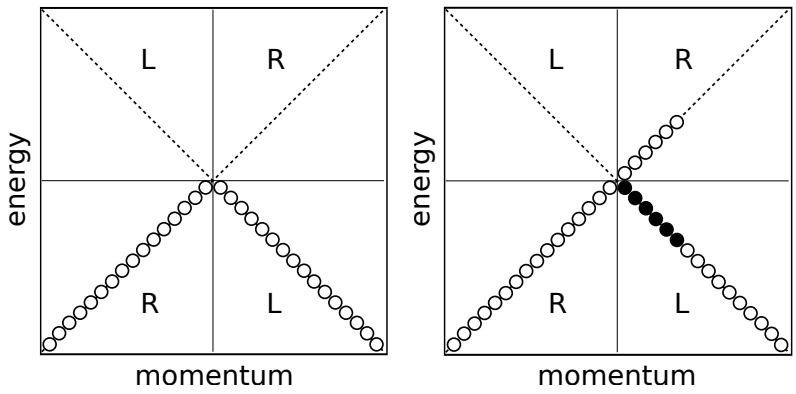

(a) before applying an electric field (b) after applying an electric field

FIG. 2. Massless fermions in the 1+1 dimension in the Dirac sea picture are shown. (a): The dispersion relation of massless fermions is linear. Before an electric field is applied, the total chirality imbalance is zero. (b): After an electric field is applied, the spectrum of fermions is shifted to the positive energy/plus momentum region, and the holes in the negative energy and positive momentum region behave as antifermions. Total chirality imbalance is produced.

III. CHIRAL TRANSPORT PHENOMENA: CHIRAL MAGNETIC EFFECT AND CHIRAL SEPARATION EFFECT

For the past decade, there has been an increasing interest in studying transport phenomena induced by anomalies, referred to as chiral transport phenomena. The most intriguing one is the chiral magnetic effect, which is the phenomenon of electric charge separation along the external magnetic field in the presence of chirality imbalance. The chiral magnetic effect has been pioneered by Vilenkin[6] and is widely known due to the work of Kharzeev *et al.* [7][8]. They presented the CME formula as below,

$$\boldsymbol{j}^V = \frac{e^2}{2\pi^2}\mu_5 \boldsymbol{B} \tag{4}$$

where $\boldsymbol{j}^V$ is the space components of the vector current(or equivalently electric current), and μ_5 is the chiral chemical potential. The chiral chemical potential μ_5 is a pseudoscalar quantity to represent an asymmetry of the chirality in the system and is conjugate to the chirality imbalance, n_5. The schematic picture of CME is shown in Fig.3. Consider the system that more right-handed fermions exist than left-handed ones; a vector current (electric current) is induced along the external magnetic field due to the spin alignment.

The chiral magnetic effect, which is the anomalous transport phenomenon as a macroscopic manifestation of the chiral anomaly, is investigated in the context of hydrodynamic in systems with massless fermions, e.g., the quark-gluon plasma in heavy-ion collisions or the Dirac/Weyl semimetals [9][10][11][12]. In noncentral heavy-ion collisions, it is believed to induce an extremely strong magnetic field, $eB \sim m_\pi^2 \sim 10^{18}$G, which is evaluated using the Lienard–Wiechert potential [13][14]. In the strong magnetic field, the CME current may induce a charge separation and an asymmetry of the charged particle distributions, which is measurable experimentally [15]. In order to detect the signal of CME currents in heavy-ion collisions, recently, isobaric ${}^{96}_{44}\mathrm{Ru} + {}^{96}_{44}\mathrm{Ru}$ and ${}^{96}_{40}\mathrm{Zr} + {}^{96}_{40}\mathrm{Zr}$ collisions at $\sqrt{s_{NN}} = 200$GeV have been conducted with analysis now underway [16][17][18][19]. The CME is a hot topic not only in high energy physics but also in the condensed matter system [12], where the massless Dirac mode has been realized in the Dirac/Weyl semimetals [20][21] and the detection of the CME current by using ultracold atoms trapped in three-dimensional optical lattices presented[22]. The experimental result for observing CME in

these systems is reported in Refs.[21], [23].

For applications of CME in the system of QCD/condensed matter, the chiral chemical potential μ_5 (or almost equivalently chirality imbalance n_5) is *a priori* assumption to investigate chiral transport phenomena. The production process of the initial chirality imbalance is, however, still in debate. For example, in the quark-gluon plasma, metastable local $\mathcal{CP}$-violating domains may be produced by transitions of the non-perturbative gluonic configurations, referred to as sphaleron transitions [8][24][25]. In Ref.[21], for the semimetal system with the electromagnetic field, the chiral chemical potential is estimated as $\mu_5 = \hbar v_F(\frac{3e^2}{4}\boldsymbol{E}\cdot\boldsymbol{B}\tau)$, where τ is the relaxation time of the chirality imbalance. In our opinion, it is essential to calculate the appearance of chirality imbalance and chirality magnetic effect with the field theoretical method without any assumptions of an initial chirality imbalance.

Another interesting anomalous transport phenomenon is the chiral separation effect (CSE), which is the generation of axial-vector current along the direction of the magnetic field[26][27]. The CSE formula is represented by

$$\boldsymbol{j}^A = \frac{\mu}{2\pi^2}\boldsymbol{B} \tag{5}$$

where μ is the chemical potential and $\boldsymbol{j}^A$ is the space component of the axial-vector current interpreted as the expectation value of spin. It is thought that the CSE formula is a chiral dual version of the CME formula, Eq.(4). The schematic piture of CSE is shown in Fig.4. In a system with a finite number of fermions, axial-vector currents (spin currents) are induced along the external magnetic field because plus(minus)-charged fermions have parallel(antiparallel) spin to the external magnetic field.

The chiral separation effect has been discussed in the context of a dense QCD system under a strong magnetic field such as compact stars. The role of CSE currents in the quark-gluon plasmas produced in heavy-ion collisions also has been attracting attention in recent years. This is because that chiral separation effect causes a gapless collective mode in the presence of an external magnetic field by interacting chiral magnetic effect, referred to as chiral magnetic wave (CMW) [28] [29]. The signal of CMW has been reported in Ref.[30]. So a comprehensive analysis that takes into account not only CME but also CSE is important.

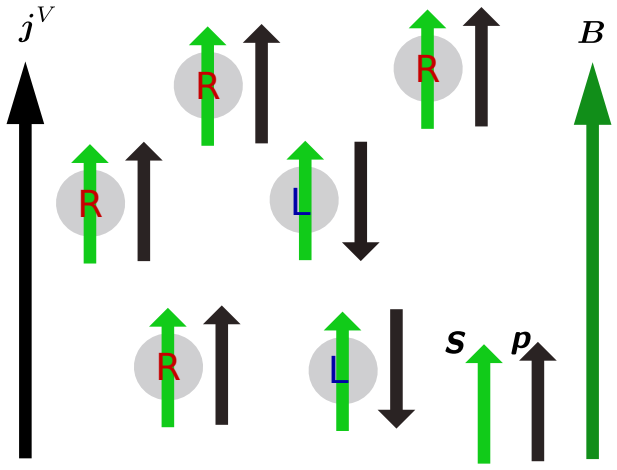

FIG. 3. The schematic picture of the chiral magnetic effect is shown. In this figure, there are more right-handed fermions than left-handed ones. In the presence of chirality imbalance, vector current (electric current) is induced along the external magnetic field due to the spin alignment.

The CME formula (4) is significant in that it suggests the occurrence of macroscopic transport phenomena due to the chiral anomaly. From a theoretical view, however, the CME current in equilibrium systems needs to be handled with care since the introduction of chiral chemical potential μ_5 in the equilibrium system is a subtle issue. It is pointed out that a CME current is forbidden in the equilibrium system, but a CSE current is allowed[31][32]. There are also some cautions from theorerical calculations according to the CME current [33][34][35][36][37]. It seems that the introduction of the chiral chemical potential implicitly assumes a system out of equilibrium [38]. In order to clarify this problem, it is crucial to explicitly calculate the time evolution of chirality imbalance within a specific model and compare their characteristic timescales[2].

The fermion mass dependence of the CME and CSE currents is also significant because the chirality imbalance strongly depends on the fermion mass. The massless fermion can be easily handled since right- and left-handed spinors are separated in the equation of motions. The mass correction to the CSE formula is discussed in Ref.[39]. In the next chapter, the mass effects of chiral anomaly and chiral transport phenomena are discussed in the view of pair productions by external electric fields.

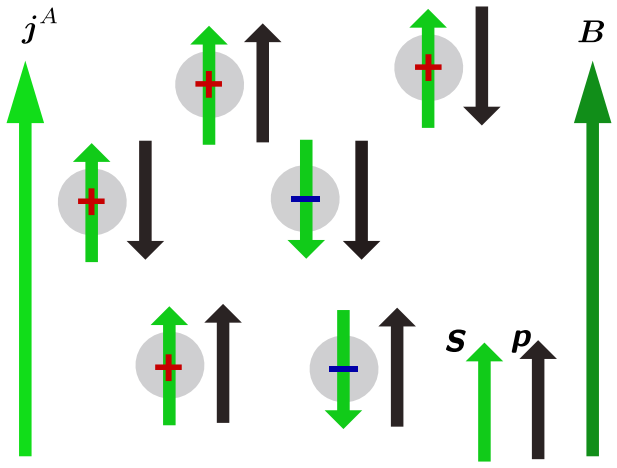

FIG. 4. The schematic picture of the chiral separation effect is shown. In this figure, there are more plus-charged fermons than minus-charged fermions. In the presence of the total fermion number, axial-vector current (spin current) is induced along the external magnetic field because a plus(minus)-charged fermion has parallel(antiparalle) spin to the external magnetic field.

IV. SCHWINGER PAIR PRODUCTION

Shortly after the Dirac equation was first formulated, in 1929, Klein was the first to imply the production of electron-positron pairs from a vacuum in the presence of a strong classical electric field[40]. In the context of relativistic quantum mechanics, tunneling from a positive frequency state to a negative frequency state can occur in a potential barrier. Even if the potential is smoothed out, the tunneling can occur, shown by Sauter[41]. The tunneling is a paradox in single-particle theory, which is later called Klein's paradox. This paradox is justified by the field theoretic interpretation.

In QED, the phenomenon is understood as particle-antiparticle pair production from the vacuum, indicated by Heisenberg and Euler first[42]. They found the 1-loop effective action of QED by integrating out a massive fermion for a constant electromagnetic field. The effective action of the background electromagnetic fields has an imaginary part, which means a vacuum in an electric field is unstable against the production of particle-antiparticle pairs from the Dirac sea.

In 1951, Schwinger gave a complete treatment of the effect using the proper time method[43], and thus the particle production in a classical electric field is called Schwinger pair production. He also computed the pair production rate per unit volume and time in a spatial-homogeneous static electric field,

$$w \sim \exp\left(-\frac{\pi m^2}{eE}\right) \tag{6}$$

The formula implies that the vacuum becomes unstable above the critical electric field, $eE_c \sim m^2$. The production rate is exponentially suppressed by the mass of fermions (in the case of QED, the fermions are electron and positron). Another point worth noting is that the formula is non-analytic in the coupling e. The dependence of eE indicates the nonperturbative nature of the Schwinger pair production.

Despite theoretical predictions from decades ago, the Schwinger pair production has yet to be experimentally observed. This is because the strength of the critical electric field for electron-positron pair productions is enormous, $E_C \sim 10^{18}$ V/m. A number of attempts have been made to detect the Schwinger pair productions. These include laser physics, heavy-ion collision experiments, and condensed matter physics. In the strong

intensity laser physics, the corresponding critical laser intensity for electron-positron pair productions is $I_C \sim 10^{29}$ W/cm^2. However, the most powerful state-of-the-art lasers just reachs about 10^{23} W/cm^2. In order to realize more powerful ultra-intense lasers, several facilities are under construct, such as the Extreme Light Infrastructure (ELI), the Exawatt Center for Extreme Light Studies (XCELS), and the High Power Laser Energy Research (HiPER), in which the intensity is expected to be 10^{26} W/cm^2. In heavy-ion collisions, it is thought that the strength of electric fields reachs to the same order of magnetic fields, $eE \sim m_\pi^2 = 10^{23}$ V/m, but the detection is yet to be. For a review[44], particle productions in heavy-ion collisions are discussed in detail. Schwinger pair production has been investigated in the context of condensed matter physics such as Superconductor[45], Mott insulator[46][47][48], and graphenes[49]. In condensed matter physics, the analogy between the energy gap and the mass gap plays an important role. It is attracting attention as experimentally achievable because the critical electric field strength for pair production is relatively small. In a time-dependent electric field, the Schwinger pair production is anolog to the Landau-Zener transition.

The connection between Schwinger pair production and chiral anomaly is of importance. In a parallel electric and magnetic field, the production rate of chirality imbalance can be related to the Schwinger pair production rate. In the view of productions of chirality imbalance by an external electromagnetic field, Landau quantization caused by an external magnetic field and Schwinger pair production by an external electric field play important roles to understand the chiral anomaly.

As is widely known, Landau quantization occurs under a magnetic field background. The continuous transverse momentum of fermions is replaced by the discrete integer, $p_T = p_x^2 + p_y^2 \to 2|eB|n$, where $n = 0, 1, 2 \ldots$ is called Landau level. At the lowest Landau level, $n = 0$, the spin-degeneracy is resolved, i.e., there are only fermions(antifermions) with spins parallel(antiparallel) to the magnetic field. In contrast, the spin-degeneracy remains in the higher Landau level, $n \geq 1$, as like the free theory. The chirality imbalance is characterized by fermions(antifermions) behavior at the lowest Landau level because the presence of spin-degeneracy causes the cancellation of spins in the higher Landau level.

As mentioned above, in the view of chirality imbalance, we just focus on the motion

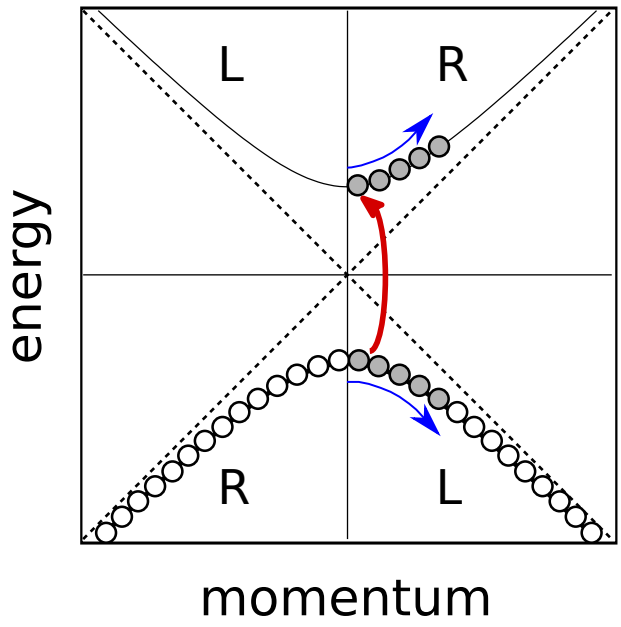

FIG. 5. The dispersion relation and pair-production of massive fermions at the lowest Landau level in the 1+3 dimensional system (or the 1+1 dimensional system) in the Dirac sea picture is shown. In a strong electric field, pair productions and acceralations occur nonadiabatically. As like the case of massless fermions, excited fermions with positive momentum and the corresponding holes contribute to the net chirality imbalance.

of fermions(antifermions) at the lowest Landau level. An external electric field, which is parallel to a magenetic field background, has two important roles; pair productions and acceralations. In a strong electric field above the energy gap (in the case of QED, the energy gap is the electron mass), the transitions from the negative energy region to the positive energy one occur nonadiabatically. Even if fermions are massive, as like the case of massless fermions, excited fermions with positive momentum and the corresponding holes contribute to the net chirality imbalance. In Fig.[5], the schematic picture of pair productions and acceralations by a strong electric field is shown.

There have been many theoretical approaches to Schwinger pair production: for a review[50], the worldline instantons formalism, the S-matrix method, the kinetic method such as the quantum Vlasov equation, the real-time Dirac-Heisenberg-Wigner (DHW) formalism, the computational quantum field theory and so on.

In this study, we investigate the relation between Schwinger pair production and chiral

anomalous transport phenomena for massive and massless fermions. We use the Bogoliubov transformation method[51]. As mentioned above, a perturbative way does not suit for the description of Schwinger pair productions and a nonperturbative way is needed. Using this method, we can treat pair-productions under strong electric fields without relying on perturbation theory. Moreover, we can obtain the time-dependent momentum distribution of pair produced pariticles. The anomaly relation tells us the macroscopic information of the system but gives us no microscopic behavior. The Bogoliubov method is helpful to understand the nonperturbative nature of chiral anomaly from microscopic views.

Another merit of the Bogoliubov method is that it suits to describe out-of-equilibrium processes. In a strong electric field, the vacuum state of fermion is unstable against pair production. This means that a certain state before the application of an electric field will change significantly after the field applied. Recent studies show that the Schwinger-Keldysh formalism gives the same results as the Bogoliubov method[38][52].

V. DIRAC EQUATION IN PARALLEL ELECTRIC AND MAGNETIC FIELDS

A. Gauge field and Dirac operator

We start from the Dirac equation in the electromagnetic field,

$$i\partial_t\psi = \hat{H}_D\psi, \tag{7}$$

$$\hat{H}_D = \hat{\mathbf{\Pi}}\cdot\boldsymbol{\alpha} + m\beta + e\phi \tag{8}$$

where $\hat{\mathbf{\Pi}} = -i\nabla - e\boldsymbol{A}$ and $(\phi, \boldsymbol{A})$ is four-potential and m is the fermion mass.

In this work, we assume external parallel electromagnetic fields along the z-direction as $\boldsymbol{E} = (0, 0, E(t)), \boldsymbol{B} = (0, 0, B)$, to produce the chirality imbalance dynamically [53][54]. The magnetic field is assumed to be spatially uniform and time-independent. On the other hand, we assume spatially uniform but time-dependent electric field $E(t)$. We choose the corresponding gauge field as, $A^\mu = (0, 0, Bx, A(t))$, where $A(t)$ is an arbitrary time-dependent real function. We only impose a constraint for an initial condition,

$$\lim_{t\to-\infty} A(t) = 0. \tag{9}$$

Correnponding initial condition for the electric field $E(t) = -\dot{A}(t)$ is written by,

$$\lim_{t\to-\infty} E(t) = 0. \tag{10}$$

This condition is usuful to define the one-particle state of the fermion at $t \to -\infty$. On the other hand, we assume the following boundary condition at $t \to \infty$,

$$\lim_{t\to\infty} A(t) = constant. \tag{11}$$

For a given time-dependent function of $A(t)$ with these boundary conditions, we can solve the Dirac equation numerically without approximations as shown later. In the previous work[2], we adopt the Sauter-type time-dependence $A(t) = E\tau(\tanh(t/\tau) + 1)$, which is non-zero at $t \to \infty$, $A(t \to \infty) \neq 0$. Here, we will develop a generalized treatment with these condtions, in which the Dirac equation reduces to the 2-component equations.

In the chiral representation of gamma matrices, the Dirac operator, H_D, is explcitly

given by

$$\hat{H}_D = \begin{pmatrix} -\hat{\Pi}_z & -(\hat{\Pi}_x - i\hat{\Pi}_y) & m & 0 \\ -(\hat{\Pi}_x + i\hat{\Pi}_y) & \hat{\Pi}_z & 0 & m \\ m & 0 & \hat{\Pi}_z & \hat{\Pi}_x - i\hat{\Pi}_y \\ 0 & m & \hat{\Pi}_x + i\hat{\Pi}_y & -\hat{\Pi}_z \end{pmatrix}. \tag{12}$$

In this paper, we assume $eB > 0$ for simplicity. The transverse mechanical momentum operators, $\hat{\Pi}_x \pm i\hat{\Pi}_y$, are explcitly written by

$$\begin{aligned} \hat{\Pi}_x + i\hat{\Pi}_y &= -i\sqrt{2|eB|}\frac{1}{\sqrt{2}}(\sqrt{|eB|}x - \frac{\hat{p}_y}{\sqrt{|eB|}} + i\frac{\hat{p}_x}{\sqrt{|eB|}}), \\ \hat{\Pi}_x - i\hat{\Pi}_y &= i\sqrt{2|eB|}\frac{1}{\sqrt{2}}(\sqrt{|eB|}x - \frac{\hat{p}_y}{\sqrt{|eB|}} - i\frac{\hat{p}_x}{\sqrt{|eB|}}). \end{aligned} \tag{13}$$

We emphasize here that the operators, $\hat{\Pi}_x \pm i\hat{\Pi}_y$, play roles of the lowering and raising operators for the harmonic oscillator, which are defined by

$$\begin{aligned} \hat{a} &= \frac{1}{\sqrt{2}}(\sqrt{|eB|}x - \frac{\hat{p}_y}{\sqrt{|eB|}} + i\frac{\hat{p}_x}{\sqrt{|eB|}}), \\ \hat{a}^\dagger &= \frac{1}{\sqrt{2}}(\sqrt{|eB|}x - \frac{\hat{p}_y}{\sqrt{|eB|}} - i\frac{\hat{p}_x}{\sqrt{|eB|}}), \end{aligned} \tag{14}$$

which satisfy the commutation relation, $[\hat{a}, \hat{a}^\dagger] = 1$. By using the bosonic lowering/raising operators, $\hat{a}, \hat{a}^\dagger$, the Dirac operator, $\hat{H}_D$, can be rewritten as follows,

$$\hat{H}_D = \begin{pmatrix} -\hat{\Pi}_z & -i\sqrt{2|eB|}\hat{a}^\dagger & m & 0 \\ i\sqrt{2|eB|}\hat{a} & \hat{\Pi}_z & 0 & m \\ m & 0 & \hat{\Pi}_z & i\sqrt{2|eB|}\hat{a}^\dagger \\ 0 & m & -i\sqrt{2|eB|}\hat{a} & -\hat{\Pi}_z \end{pmatrix}. \tag{15}$$

This implies that solutions of the Dirac Hamiltonian are just eigenfunctions of the bosonic number operators, which will be desicussed in the next section.

B. Solutions of Dirac equation

We consider solutions in a finite volume system, $V = L_x L_y L_z$, for later convenience. Infinite volume limit, $V \to \infty$, is taken after calculating observables.

In previous works[2][54], the Dirac equation in parallel electric and magnetic fields was solved via the squared Dirac equation. In this paper, we use the form of the solution known from previous works for the space-dependent part and consider solving the first-order equation for the time-dependent part. The solution of Eq.(7), called mode-function, is expanded as follows,

$$\psi_{n,n_z,n_y}(t,\boldsymbol{x}) = Ne^{ik_y y+ik_z z}G_{n,n_y}(x)\psi_{n,n_z}(t) \tag{16}$$

where $k_y = 2\pi n_y/L_y, k_z = 2\pi n_z/L_z$ with n_y and n_z. We introduce the diagonalized matrix, $G_{n,n_y}(x)$, as follows,

$$G_{n,n_y}(x) = \mathrm{diag}(g_{n,n_y}(x), g_{n-1,n_y}(x), g_{n,n_y}(x), g_{n-1,n_y}(x)) \tag{17}$$

Here, $g_{n,n_y}(x)$ is the non-dimensional eigenfunction of the bosonic number operator, $\hat{a}^\dagger\hat{a}$, referred to as Landau levels,

$$g_{n,n_y}(x) = \frac{1}{\sqrt{2^n n!}}\left(\frac{1}{\pi}\right)^{1/4} H_n(\sqrt{|eB|}x - \frac{k_y}{\sqrt{|eB|}})\exp\left(-(\sqrt{|eB|}x - \frac{k_y}{\sqrt{|eB|}})^2/2\right) \tag{18}$$

where $n = 0, 1, 2\ldots$ and $\mathcal{N} = \frac{eBL_xL_y}{2\pi}$ is the degeneracy of Landau level. The normalization factor, N, is determined later. We set the time-dependent part, $\psi_{n,n_z}(t)$, as dimensionless four-spinor, in other words, the normalization factor, N, has mass dimension 3/2.

This eigenfunction satisfies the orthonormal relation and the completeness relation,,

$$\int dx g_{n,n_y}(x)g_{n',n_y}(x) = \frac{1}{\sqrt{|eB|}}\delta_{nn'}, \tag{19}$$

$$\sum_{n=0}^{\infty} g_{n,n_y}(x)g_{n,n_y}(x') = \sqrt{|eB|}\delta(x-x'). \tag{20}$$

Note that the orthonormality should be justified when $|x| \to \infty$.

The lowest Landau level

We next solve the time-dependent part of the Dirac equation for ψ obtained from (12) and (16). For the lowest Landau level(LLL), $n = 0$, we merely consider only the 1st and 3rd component of the time-dependent part, $\psi^{(1)}_{n,n_z}(t), \psi^{(3)}_{n,n_z}(t)$ because of $g_{-1,n_y}(x) = 0$,

$$i\partial_t \begin{pmatrix} \psi^{(1)}_{0,n_z}(t) \\ \psi^{(3)}_{0,n_z}(t) \end{pmatrix} = \begin{pmatrix} -k_z + eA(t) & m \\ m & k_z - eA(t) \end{pmatrix} \begin{pmatrix} \psi^{(1)}_{0,n_z}(t) \\ \psi^{(3)}_{0,n_z}(t) \end{pmatrix} \tag{21}$$

We then obtain the mode-function for the lowest Landau level,

$$\psi_{0,n_z,n_y}(t,\boldsymbol{x}) = \exp(ik_y y + ik_z z)\begin{pmatrix} g_{0,n_y}(x)\psi^{(1)}_{0,n_z}(t) \\ 0 \\ g_{0,n_y}(x)\psi^{(3)}_{0,n_z}(t) \\ 0 \end{pmatrix} \tag{22}$$

As expected, this solution is eigenstate of $\Sigma_3 = \gamma^3\gamma^5$, that is ,

$$\Sigma_3\psi_{0,n_z,n_y}(t,\boldsymbol{x}) = +\psi_{0,n_z,n_y}(t,\boldsymbol{x}) \tag{23}$$

which imlies that the spin-up (spin-down) state is allowed for the positive (negative) energy particle in the lowest Landau level.

The higher Landau level

For the higher Landau level, $n \geq 1$, the mode-function $\psi_{n,n_z}(t)$, follows the equation,

$$i\partial_t\psi_{n,n_z}(t) = H_D(n,n_z)\psi_{n,n_z}(t) \tag{24}$$

where

$$H_D(n,n_z) = \begin{pmatrix} -k_z + eA(t) & i\sqrt{2eBn} & m & 0 \\ -i\sqrt{2eBn} & k_z - eA(t) & 0 & m \\ m & 0 & k_z - eA(t) & -i\sqrt{2eBn} \\ 0 & m & i\sqrt{2eBn} & -k_z + eA(t) \end{pmatrix}. \tag{25}$$

This Hamiltonian can be block-diagonalized by an unitary matrix, U, as follows

$$H_D^{'}(n,n_z) = UH_D(n,n_z)U^\dagger = \begin{pmatrix} \boldsymbol{h}_{n,n_z}\cdot\boldsymbol{\sigma} & 0 \\ 0 & \boldsymbol{h}_{n,n_z}\cdot\boldsymbol{\sigma} \end{pmatrix} \tag{26}$$

where

$$\boldsymbol{h}_{n,n_z} = (\sqrt{m^2 + 2|eB|n},\ 0,\ \ -k_z + eA(t)), \tag{27}$$

and

$$U = \frac{1}{\sqrt{2}}\begin{pmatrix} \sigma_y & \sigma_x \\ -i\sigma_z & \sigma_0 \end{pmatrix}\mathrm{diag}(\mathrm{e}^{-i\lambda/2}, \mathrm{e}^{i\lambda/2}, \mathrm{e}^{i\lambda/2}, \mathrm{e}^{-i\lambda/2}), \tag{28}$$

$$\lambda = \arctan\left(\frac{\sqrt{2|eB|n}}{m}\right). \tag{29}$$

Now the equaion to be solved comes down to the following two-component equation,

$$i\partial_t \phi_{n,n_z} = \boldsymbol{h}_{n,n_z} \cdot \boldsymbol{\sigma} \phi_{n,n_z}. \tag{30}$$

Such two-component equations are widely found in the physics of two-level systems such as magnetic moments in the magnetic fields, the solutions of Eq.(24) can be written simply with the two-component spinor,

$$\psi_{n,n_z}(t) = U \begin{pmatrix} \xi_1 \phi_{n,n_z}(t) \\ \xi_2 \phi_{n,n_z}(t) \end{pmatrix} = U\xi \otimes \phi, \tag{31}$$

where ξ_1, ξ_2 are arbitrary constants, and $\xi = (\xi_1, \xi_2)^t$. Apparently, the solution for higher Landau levels processes four independant degrees of freedom contrary to the LLL solutions in Eq.(22).

C. Positive and negative energy solutions and spin degree of freedom

To determine the positive and negative energy solutions of Eq.(30), we consider the asymptotic limit, $t \to -\infty$. By virtue of the condtion Eq.(9), positive and negative energy solutions of Eq.(30), $\phi^{(+)}$ and $\phi^{(-)}$ should coincide with the orthonormal plane wave solutions

$$\phi^{(+)}_{n,n_z} \xrightarrow[t\to-\infty]{} \mathrm{e}^{-i\omega_{n,n_z}t} \begin{pmatrix} \cos(\rho/2) \\ -\sin(\rho/2) \end{pmatrix}, \tag{32}$$

$$\phi^{(-)}_{n,n_z} \xrightarrow[t\to-\infty]{} \mathrm{e}^{+i\omega_{n,n_z}t} \begin{pmatrix} \sin(\rho/2) \\ \cos(\rho/2) \end{pmatrix}. \tag{33}$$

where the energy at $t \to -\infty$ is given by $\omega_{n,n_z} = \sqrt{m^2 + k_z^2 + 2eBn}$ and the phase is $\rho = \arctan\Big(k_z/\sqrt{m^2 + 2eBn}\Big)$. It is important to note that relations between positive and negative energy solutions are given by $\phi^{(-)}_{n,n_z} = \Theta\phi^{(+)}_{n,n_z}, \phi^{(+)}_{n,n_z} = -\Theta\phi^{(-)}_{n,n_z}$, where $\Theta = i\sigma_y K$ is time-reversal conjugation operator and K is complex conjugation operator. They imply that a negative charged state can be interpreted as the corresponding time-reversal positive charged one. Hense, we can express solutions of the two component spinor by single

function ϕ_{n,n_z} using relations,

$$\begin{aligned}\phi^{(+)}_{n,n_z}(t) &= \phi_{n,n_z}(t),\\ \phi^{(-)}_{n,n_z}(t) &= \Theta\phi_{n,n_z}(t).\end{aligned} \tag{34}$$

The positive and negative solution satisfy the orthonormal condition,

$$|\phi^{(\pm)}_{n,n_z}|^2 = |\phi_{n,n_z}|^2 = 1, \tag{35}$$

$$\phi^{\dagger(\pm)}_{n,n_z}\phi^{(\mp)}_{n,n_z} = (\Theta\phi_{n,n_z})^\dagger\phi_{n,n_z} = \phi^\dagger_{n,n_z}\Theta\phi_{n,n_z} = 0. \tag{36}$$

Next, we determine the spin structure of the solutions. In the heavy mass limit, $m \gg \sqrt{2eBn}$ and $\lambda \to \frac{\pi}{2}$, ψ may reduce to the non-relativestic spinor, if we choose ξ properly. This can be done by choosing $\xi = (\mathrm{e}^{i\lambda/2}/\sqrt{2}, -i\mathrm{e}^{-i\lambda/2}/\sqrt{2})$ and $\Theta\xi = (-i\mathrm{e}^{i\lambda/2}/\sqrt{2}, \mathrm{e}^{-i\lambda/2}/\sqrt{2})$. In fact, time-dependent parts of the solutions become

$$\psi^{(\pm)}_{n,n_z}(t) = \begin{pmatrix}\phi^{(\pm)}_1\\ i\sin(\lambda)\phi^{(\pm)}_2\\ \cos(\lambda)\phi^{(\pm)}_2\\ 0\end{pmatrix} \xrightarrow[m\to\infty]{} \begin{pmatrix}\phi^{(\pm)}_1\\ 0\\ \phi^{(\pm)}_2\\ 0\end{pmatrix} \tag{37}$$

$$\psi^{(\pm)}_{n,n_z}(t) = \begin{pmatrix}0\\ \cos(\lambda)\phi^{(\pm)}_2\\ i\sin(\lambda)\phi^{(\pm)}_2\\ \phi^{(\pm)}_1\end{pmatrix} \xrightarrow[m\to\infty]{} \begin{pmatrix}0\\ \phi^{(\pm)}_2\\ 0\\ \phi^{(\pm)}_1\end{pmatrix} \tag{38}$$

We finally arrive at expressions for the solutions, $\psi^{(u,\sigma)}_{n,n_z,n_y}$, where $u = +/-$ denotes the

positive/negative energy and $\sigma = \uparrow / \downarrow$ represents spin up/down state, respectively.

$$\psi^{(+,\uparrow)}_{n,n_z,n_y}(t,\boldsymbol{x}) = N\exp(ik_y y + ik_z z)\begin{pmatrix} g_{n,n_y}(x)\phi_1^{(+)} \\ i\sin(\lambda)g_{n-1,n_y}(x)\phi_2^{(+)} \\ \cos(\lambda)g_{n,n_y}(x)\phi_2^{(+)} \\ 0 \end{pmatrix}, \tag{39}$$

$$\psi^{(+,\downarrow)}_{n,n_z,n_y}(t,\boldsymbol{x}) = N\exp(ik_y y + ik_z z)\begin{pmatrix} 0 \\ \cos(\lambda)g_{n-1,n_y}(x)\phi_2^{(+)} \\ i\sin(\lambda)g_{n,n_y}(x)\phi_2^{(+)} \\ g_{n-1,n_y}(x)\phi_1^{(+)} \end{pmatrix}, \tag{40}$$

$$\psi^{(-,\downarrow)}_{n,n_z,n_y}(t,\boldsymbol{x}) = N\exp(ik_y y + ik_z z)\begin{pmatrix} g_{n,n_y}(x)\phi_1^{(-)} \\ i\sin(\lambda)g_{n-1,n_y}(x)\phi_2^{(-)} \\ \cos(\lambda)g_{n,n_y}(x)\phi_2^{(-)} \\ 0 \end{pmatrix}, \tag{41}$$

$$\psi^{(-,\uparrow)}_{n,n_z,n_y}(t,\boldsymbol{x}) = N\exp(ik_y y + ik_z z)\begin{pmatrix} 0 \\ \cos(\lambda)g_{n-1,n_y}(x)\phi_2^{(-)} \\ i\sin(\lambda)g_{n,n_y}(x)\phi_2^{(-)} \\ g_{n-1,n_y}(x)\phi_1^{(-)} \end{pmatrix} \tag{42}$$

If we take $n = 0$, eqs.(39)-(42) reduce to the LLL solutions Eq.(22). As expected, we find

$$\psi^{(+,\downarrow)}_{0,n_z,n_y}(t,\boldsymbol{x}) = \psi^{(-,\uparrow)}_{0,n_z,n_y}(t,\boldsymbol{x}) = 0. \tag{43}$$

since $g_{n-1} = 0$ and $\lambda = 0$ for $n = 0$.

By using the orthonormal and completeness realtion of the Hermite polynomials and plane-wave and taking the normalization factor $N = (eB)^{1/4}/\sqrt{L_y L_z}$, we obtain the orthonormal relation,

$$\int d^3x \psi^{\dagger(u,\sigma)}_{n,n_y,n_z}(t,\boldsymbol{x})\psi^{(u',\sigma')}_{n',n'_y,n'_z}(t,\boldsymbol{x}) = \delta_{uu'}\delta_{\sigma\sigma'}\delta_{nn'}\delta_{n_y n'_y}\delta_{n_z n'_z} \tag{44}$$

and completeness relation,

$$\sum_{u=\pm}\sum_{\sigma=\uparrow,\downarrow}\sum_{n=0}^{\infty}\sum_{n_y=-\mathcal{N}/2}^{\mathcal{N}/2}\sum_{n_z=-\infty}^{\infty}[\psi^{(u,\sigma)}_{n,n_y,n_z}(t,\boldsymbol{x})]_\alpha[\psi^{\dagger(u,\sigma)}_{n,n_y,n_z}(t,\boldsymbol{x}')]_\beta = \delta_{\alpha\beta}\delta^{(3)}(\boldsymbol{x}-\boldsymbol{x}'). \tag{45}$$

where α, β are spinor indices. Strictly speaking, the orthonormal and completeness relation are satisfied only if taking infinite volume limit, $V \to \infty$.

VI. QUANTIZATION AND EXPECTATION VALUES

A. Canonical quantization and finite Fermi energy system

In the previous section, we obtained the solutions of the Dirac equation which satisfy the complete-orthonormal relation. Using these solutions, we expand the fermionic field operator as,

$$\hat{\psi}(x) = \sum_{n=0}^{\infty} \sum_{n_y=-\mathcal{N}/2}^{\mathcal{N}/2} \sum_{n_z=-\infty}^{\infty} \sum_{\sigma=\uparrow,\downarrow} (\hat{b}_{\sigma,\boldsymbol{n}} \psi_{\boldsymbol{n}}^{(+,\sigma)}(t,\boldsymbol{x}) + \hat{d}^{\dagger}_{-\sigma,-\boldsymbol{n}} \psi_{\boldsymbol{n}}^{(-,-\sigma)}(t,\boldsymbol{x})) \tag{46}$$

where the coefficients, $\hat{b}_{\sigma,n,n_y,n_z}, \hat{d}^{\dagger}_{-\sigma,n,-n_y,-n_z}$, are dimensionless constants. Note that $\hat{b}_{\downarrow,0,n_y,n_z}, \hat{d}^{\dagger}_{\uparrow,0,-n_y,-n_z}$ do not exist because of Eq.(43).

The field operator is quantized by requiring the canonical anti-commutation relation,

$$\begin{aligned} &\{\hat{\psi}_\alpha(t,\boldsymbol{x}), \hat{\psi}^{\dagger}_\beta(t,\boldsymbol{x}')\} = \delta_{\alpha\beta}\delta(\boldsymbol{x}-\boldsymbol{x}'), \\ &\{\hat{\psi}_\alpha(t,\boldsymbol{x}), \hat{\psi}_\beta(t,\boldsymbol{x}')\} = \{\hat{\psi}^{\dagger}_\alpha(t,\boldsymbol{x}), \hat{\psi}^{\dagger}_\beta(t,\boldsymbol{x}')\} = 0, \end{aligned} \tag{47}$$

Eq.(47) is equavalent to anti-commutation relations for expansion coefficients,

$$\{\hat{b}_{\sigma,\boldsymbol{n}}, \hat{b}^{\dagger}_{\sigma',\boldsymbol{n}'}\} = \{\hat{d}_{\sigma,\boldsymbol{n}}, \hat{d}^{\dagger}_{\sigma',\boldsymbol{n}'}\} = \delta_{\sigma\sigma'}\delta_{nn'}\delta_{n_y n_y'}\delta_{n_z n_z'}, \text{ otherwise zero} \tag{48}$$

where $\hat{b}_{\sigma,\boldsymbol{n}}, \hat{d}_{\sigma,\boldsymbol{n}}$ are interpreted as annihilation operators of fermions/antifermions respectively. The vacuum state is defined by,

$$\hat{b}_{\sigma,\boldsymbol{n}} |0\rangle = 0, \ \hat{d}_{\sigma,\boldsymbol{n}} |0\rangle = 0 \text{ (for all } \sigma, \boldsymbol{n}) \tag{49}$$

with the normalization $\langle 0|0\rangle = 1$. We define the vacuum state $|0\rangle$ at $t \to -\infty$ in the Heisenberg picture, that is, $|0\rangle$ is time-independent state. The finite Fermi energy system, in which the positive energy states are filled up to a certain maximum of the single particle energy (Fermi energy, E_F) is constructed by multiplying the creation operators to the vacuum state,

$$|F\rangle = \prod_{\substack{\omega_{n,n_z} \le E_F, \\ \sigma=\uparrow,\downarrow}} \hat{b}^{\dagger}_{\sigma,\boldsymbol{n}} |0\rangle \tag{50}$$

B. Vacuum expectation values

The Hamiltonian density operator, $\hat{\mathcal{H}}(t)$, is given by

$$\hat{\mathcal{H}}(t) \equiv \frac{1}{V}\int_V \mathrm{d}^3x \frac{1}{2}\Big[\hat{\psi}^\dagger(x), \hat{H}_D\hat{\psi}(x)\Big] \tag{51}$$

The fermionic field operator satisfies the Heisenberg equation, $i\frac{\mathrm{d}}{\mathrm{d}t}\hat{\psi}(t) = [\psi(t), \hat{\mathcal{H}}(t)]$. The Hamiltonian is explcitly written with the creation/annihilation operators,

$$\begin{aligned}\hat{\mathcal{H}}(t) = \frac{1}{V}\sum_{\sigma=\uparrow,\downarrow}\sum_{n=0}^{\infty}\sum_{n_y=-\mathcal{N}/2}^{\mathcal{N}/2}\sum_{n_z=-\infty}^{\infty}&[\epsilon_{n,n_z}(t)(\hat{b}^\dagger_{\sigma,\boldsymbol{n}}\hat{b}_{\sigma,\boldsymbol{n}} + \hat{d}^\dagger_{-\sigma,-\boldsymbol{n}}\hat{d}_{-\sigma,-\boldsymbol{n}} - 1)\\ &+ \gamma_{n,n_z}(t)\hat{b}_{\sigma,\boldsymbol{n}}\hat{d}_{-\sigma,-\boldsymbol{n}} + \gamma^*_{n,n_z}(t)\hat{d}^\dagger_{-\sigma,-\boldsymbol{n}}\hat{b}^\dagger_{\sigma,\boldsymbol{n}}] \qquad (52)\\ = \frac{1}{V}\sum_{\sigma=\uparrow,\downarrow}\sum_{n=0}^{\infty}\sum_{n_y=-\mathcal{N}/2}^{\mathcal{N}/2}\sum_{n_z=-\infty}^{\infty}&\boldsymbol{a}_{n,n_z}\cdot\hat{\boldsymbol{\tau}}_{\sigma,\boldsymbol{n}} \qquad (53)\end{aligned}$$

where the coefficients are given by

$$\epsilon_{n,n_z}(t) = \phi^\dagger_{n,n_z}(t)\boldsymbol{h}_{n,n_z}(t)\cdot\boldsymbol{\sigma}\phi_{n,n_z}(t) \tag{54}$$

$$\gamma_{n,n_z}(t) = -(\Theta\phi_{n,n_z}(t))^\dagger\boldsymbol{h}_{n,n_z}(t)\cdot\boldsymbol{\sigma}\phi_{n,n_z}(t) \tag{55}$$

The last equality (53) is the pseudospin representation [55][56][57][58][45] where is a vector with three components, $\boldsymbol{a}_{n,n_z} = (\mathrm{Re}[\gamma_{n,n_z}], \mathrm{Im}[\gamma_{n,n_z}], \epsilon_{n,n_z})$, and $\hat{\boldsymbol{\tau}}_{\sigma,\boldsymbol{n}}$ are the spin-matrix-like operators defined by

$$\begin{aligned}\hat{\tau}^1_{\sigma,\boldsymbol{n}} &= \hat{b}_{\sigma,\boldsymbol{n}}\hat{d}_{-\sigma,-\boldsymbol{n}} + \hat{d}^\dagger_{-\sigma,-\boldsymbol{n}}\hat{b}^\dagger_{\sigma,\boldsymbol{n}}\\ \hat{\tau}^2_{\sigma,\boldsymbol{n}} &= (-i)(\hat{b}_{\sigma,\boldsymbol{n}}\hat{d}_{-\sigma,-\boldsymbol{n}} - \hat{d}^\dagger_{-\sigma,-\boldsymbol{n}}\hat{b}^\dagger_{\sigma,\boldsymbol{n}})\\ \hat{\tau}^3_{\sigma,\boldsymbol{n}} &= \hat{b}^\dagger_{\sigma,\boldsymbol{n}}\hat{b}_{\sigma,\boldsymbol{n}} + \hat{d}^\dagger_{-\sigma,-\boldsymbol{n}}\hat{d}_{-\sigma,-\boldsymbol{n}} - 1\end{aligned} \tag{56}$$

which satisfy $[\hat{\tau}^i_{\boldsymbol{n}}, \hat{\tau}^j_{\boldsymbol{n}}] = i\epsilon^{ijk}\hat{\tau}^k_{\boldsymbol{n}}$. As we will discuss later, this representation is helpful to diagonalize the Hamiltonian. At $t \to -\infty$, the asymptotic Hamiltonian is

$$\hat{\mathcal{H}}(t) \xrightarrow[t\to-\infty]{} \frac{1}{V}\sum_{\sigma=\uparrow,\downarrow}\sum_{n=0}^{\infty}\sum_{n_y=-\mathcal{N}/2}^{\mathcal{N}/2}\sum_{n_z=-\infty}^{\infty}[\omega_{n,n_z}(\hat{b}^\dagger_{\sigma,\boldsymbol{n}}\hat{b}_{\sigma,\boldsymbol{n}} + \hat{d}^\dagger_{-\sigma,-\boldsymbol{n}}\hat{d}_{-\sigma,-\boldsymbol{n}} - 1). \tag{57}$$

Summing up over degenerate states, one can obtain the expectation values of Hamil-

tonian as,

$$\langle F|\,\hat{\mathcal{H}}\,|F\rangle = \frac{|eB|}{2\pi}\frac{1}{L_z}\sum_{n_z=-\infty}^{\infty}\epsilon_{0,n_z}(t)[-1+\theta(|k_z|-p_F^{(0)})] + \frac{|eB|}{2\pi}\sum_{\sigma=\uparrow,\downarrow}\sum_{n=1}^{\infty}\frac{1}{L_z}\sum_{n_z=-\infty}^{\infty}\epsilon_{n,n_z}(t)[-1+\theta(|k_z|-p_F^{(n)})] \tag{58}$$

where $\theta(|p_z|-p_F^{(n)})$ is the step-function and $p_F^{(n)}=\sqrt{E_F-m^2-2eBn}$ is the Fermi momentum at each Landau level. Taking infinite volume limit, $V\to\infty$, and $\frac{1}{L_z}\sum_{n_z=-\infty}^{\infty}\to\int\frac{dp_z}{2\pi}$, Eq.(58) becomes

$$\langle F|\,\hat{\mathcal{H}}\,|F\rangle = \frac{|eB|}{2\pi}\sum_{n=0}^{\infty}\int\frac{dp_z}{2\pi}\alpha_n\epsilon_{n,n_z}(t)[(\theta(|p_z|-p_F^{(n)})-1) \tag{59}$$

where $\alpha_n=1(n=0)$ or $2(n\geq 1)$.

In the same way, the expectation values of currents are also given by

$$\left\langle\bar{\psi}\Gamma\psi\right\rangle = \frac{1}{V}\int_V \mathrm{d}^3x\,\langle F|\,\frac{1}{2}\Big[\hat{\bar{\psi}}(x),\Gamma\hat{\psi}(x)\Big]\,|F\rangle \tag{60}$$

where Γ is an arbitrary product of gamma matrices. Taking the infinite volume limit, Eq.(60) are simply written by

$$N=\left\langle\bar{\psi}\gamma^0\psi\right\rangle = \frac{|eB|}{2\pi}\sum_{n=0}^{\infty}\int\frac{dp_z}{2\pi}\alpha_n\theta(|p_z|-p_F^{(n)}) \tag{61}$$

$$s_3=\left\langle\bar{\psi}\gamma^3\gamma^5\psi\right\rangle = \frac{p_F^{(0)}}{2\pi^2}eB \tag{62}$$

$$j_3(t)=\left\langle\bar{\psi}\gamma^3\psi\right\rangle = \frac{|eB|}{2\pi}\sum_{n=0}^{\infty}\int\frac{dp_z}{2\pi}\alpha_n\phi^\dagger_{n,p_z}\sigma_z\phi_{n,p_z}\theta(|p_z|-p_F^{(n)}) \tag{63}$$

$$n_5(t)=\left\langle\bar{\psi}\gamma^0\gamma^5\psi\right\rangle = \frac{eB}{2\pi}\int\frac{dp_z}{2\pi}\phi^\dagger_{0,p_z}\sigma_z\phi_{0,p_z}\theta(|p_z|-p_F^{(0)}) \tag{64}$$

$$\eta(t)=\left\langle\bar{\psi}i\gamma^5\psi\right\rangle = \frac{eB}{2\pi}\int\frac{dp_z}{2\pi}\phi^\dagger_{0,p_z}\sigma_y\phi_{0,p_z}\theta(|p_z|-p_F^{(0)}) \tag{65}$$

$$\chi(t)=\left\langle\bar{\psi}\psi\right\rangle = \frac{|eB|}{2\pi}\sum_{n=0}^{\infty}\int\frac{dp_z}{2\pi}\alpha_n\frac{m}{\sqrt{m^2+2|eB|n}}\phi^\dagger_{n,p_z}\sigma_x\phi_{n,p_z}\theta(|p_z|-p_F^{(n)}) \tag{66}$$

$$P_3(t)=\left\langle\bar{\psi}i\gamma^0\gamma^3\psi\right\rangle = \frac{|eB|}{2\pi}\sum_{n=0}^{\infty}\int\frac{dp_z}{2\pi}\alpha_n\frac{m}{\sqrt{m^2+2|eB|n}}\phi^\dagger_{n,p_z}\sigma_y\phi_{n,p_z}\theta(|p_z|-p_F^{(n)}) \tag{67}$$

$$M_3(t)=\left\langle\bar{\psi}i\gamma^1\gamma^2\psi\right\rangle = \frac{eB}{2\pi}\int\frac{dp_z}{2\pi}\phi^\dagger_{0,p_z}\sigma_x\phi_{0,p_z}\theta(|p_z|-p_F^{(0)}) \tag{68}$$

Other components of bilinear forms such as $\Gamma = \{\gamma^1, \gamma^2, \gamma^1\gamma^5, \gamma^2\gamma^5, i\gamma^0\gamma^1, i\gamma^0\gamma^2, i\gamma^2\gamma^3, i\gamma^3\gamma^1\}$ are always equal to zero due to the absence of electric and magnetic fields according to x, y-axis.

Due to the cancellation of up and down spin at the higher Landau levels, chirality imbalance n_5, spin expectation value s_3, pseudoscalar condensation η and magnetic dipole moment M_3 have the contribution of the lowest Landau level only. In contrast, total number density N, electric current j_3, scalar condensation χ and electric dipole moment P_3 have the contribution from all possible Landau levels.

If the Fermi energy is smaller than the magnetic field, $E_F < \sqrt{2|eB|}$, particles are occupied in only the lowest Landau level. So the total number density is equal to the total spin, except for the sign, $N = \mathrm{sgn}(eB)s_3$. If the Fermi energy is larger than the magnetic field, $E_F > \sqrt{2|eB|}$, particles are occupied in not only the lowest Landau level but also the higher Landau levels. The schematic illustration of the dispersion relation at a Fermi sphere and spin degrees of freedom in the system is shown by Fig.6.

The spin expectation value is proportional to the Fermi momentum at the lowest Landau level, $p_F^{(0)}$, and the strength of the magnetic field. Clearly, in the limit of zero Fermi energy, $E_F \to 0$, total number density and spin expectation value vanish. In contrast, the magenetic dipole moment has non-zero values even in the limit of zero Fermi energy. This difference may come from roles of antifermions for these matrix elements, the spin $\langle\bar{\psi}\gamma^3\gamma^5\psi\rangle$ express a sum of fermion and antifermion contributions, while the magenetic dipole moments $\langle\bar{\psi}i\gamma^1\gamma^2\psi\rangle$ describes their differences.

The formula of spin expectation value (62) is consistent with the previous work[26]. In massless limit, the Fermi momentum at the lowest Landau level, $p_F^{(0)}$, is equal to Fermi energy and chemical potential, $p_F^{(0)} = E_F = \mu$, so the spin expectation value becomes

$$s_3 = \frac{\mu}{2\pi^2}eB \tag{69}$$

This is the chiral separation effect in this framework.

Total number density and spin are time-independent. These are conserved quantities even applying an electric field. On the other hand, chirality imbalance, electric current, and pseudoscalar condensation are time-dependent. An applied electric field can produce these. To evaluate the evolutions properly, we need to regularize the infinite momentum

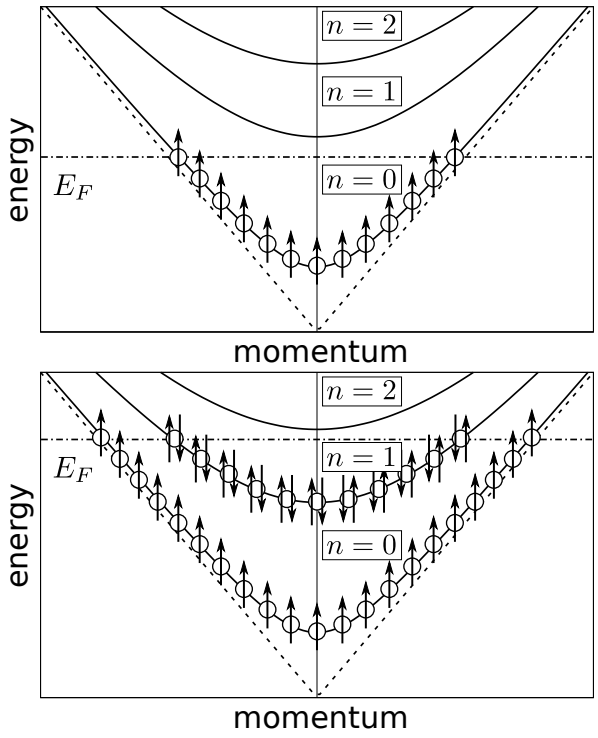

FIG. 6. The dispersion relation and schematic illustration of spin degree of freedom in the Fermi sphere, where n is the index of Landau level and E_F is the Fermi energy. In the lowest Landau level, spin degree of freedom is one, that is, only the spin aligned the magnetic field is occupied. In contrast, spin degree of freedom is two in the higher Landau level, that is, both up and down spin are occupied.

integration, discussed in the next section.

C. Regularization and anomaly relation

The contribution from the vacuum appears in the vacuum expectation values of chirality imbalance, n_5, electric current, j_3, and pseudoscalar condensation, η, so we have to evaluate the integration of momentum over an infinite interval properly. We use point-split regularization for the evaluation of vacuum expectation values in a gauge-invariant way. We consider the replacement of a local bi-linear form to a non-local one as below,

$$\bar{\psi}(z)\Gamma\psi(z) \to \lim_{\epsilon\to 0}\int \mathrm{d}z'\bar{\psi}(z)\Gamma h_\epsilon(z-z')U(z,z')\psi(z'), \tag{70}$$

where $h_\epsilon(z-z')$ is a delta-sequence function and $U(z,z')$ is the Wilson line defined as

$$\lim_{\epsilon\to 0} h_\epsilon(z-z') = \delta(z-z'), \tag{71}$$

$$U(z,z') = \exp\left[ie\int_{z'}^{z} d\tilde{z}^\mu A_\mu(\tilde{z})\right], \tag{72}$$

The Wilson line is needed for invariance of the local phase transformation $\psi \to \psi' = \mathrm{e}^{i\alpha(x)}\psi$. We consider the replacement of mode-functions for z-component only and choose the straight line as the path of the Wilson line. So one can integrate the non-local bi-linear form as below,

$$\int \mathrm{d}z'\bar{\psi}(z)\Gamma h_\epsilon(z-z')U(z,z')\psi(z') = \bar{\psi}_{n,p_z}\Gamma\tilde{h}_\epsilon(p_z-eA(t))\psi_{n,p_z}, \tag{73}$$

where $\tilde{h}_\epsilon(p_z - eA(t))$ is the Fourier coefficient of the delta-sequence function. If one chooses the sinc function, $h_\epsilon(z-z') = \frac{\sin(\pi(z-z')/\epsilon)}{\pi(z-z')}$, as delta-sequence function, the Fourier coefficient is given by box function $\tilde{h}_\epsilon(p_z - eA(t)) = \theta(|1/\epsilon| - p_z - eA(t))$. The parameter, $1/\epsilon = \Lambda$, is interpreted as the cut-off parameter according to the canonical momentum aligned z-axis, p_z. So we can obtain the regularized vacuum expectation values,

$$j_3(t) = \frac{|eB|}{2\pi}\sum_{n=0}^{\infty}\int_{-\Lambda+eA(t)}^{\Lambda-eA(t)}\frac{dp_z}{2\pi}\alpha_n\phi^\dagger_{n,p_z}(t)\sigma_z\phi_{n,p_z}(t)\theta(|p_z|-p_F^{(n)}), \tag{74}$$

$$n_5(t) = \frac{eB}{2\pi}\int_{-\Lambda+eA(t)}^{\Lambda-eA(t)}\frac{dp_z}{2\pi}\phi^\dagger_{0,p_z}(t)\sigma_z\phi_{0,p_z}(t)\theta(|p_z|-p_F^{(0)}), \tag{75}$$

$$\eta(t) = \frac{eB}{2\pi}\int_{-\Lambda+eA(t)}^{\Lambda-eA(t)}\frac{dp_z}{2\pi}\phi^\dagger_{0,p_z}(t)\sigma_y\phi_{0,p_z}(t)\theta(|p_z|-p_F^{(0)}). \tag{76}$$

With the point-split regularization, chirality imbalance n_5 satisfies the anomaly relation,

$$\partial_t n_5 = 2m\eta + \frac{e^2}{2\pi^2}BE(t), \tag{77}$$

when taking the large cut-off limit, $\Lambda\to\infty$. The anomalous term, $\frac{e^2}{2\pi^2}BE(t)$, comes from the time-dependence of the edge of ultraviolet momentum cut-off, $[-\Lambda+eA(t), \Lambda-eA(t)]$, which is the nature of the chiral anomaly. The anomaly relation is satisfied even in system with non-zero Fermi energy, which is consistent with the previous work[5].

The anomaly relation for massless fermion is also satisfied,

$$\partial_t n_5 = \frac{e^2}{2\pi^2}BE(t). \tag{78}$$

By integrating of time, we can obtain a simple form

$$n_5 = -\frac{e^2}{2\pi^2} BA(t). \tag{79}$$

The rhs of Eq.(79) is proportional to the magenetic helicity density

$$h(t) = \frac{1}{V}\int d^3x \boldsymbol{A}\cdot\boldsymbol{B}. \tag{80}$$

which relates to the winding number of a magnetic field.

The proof of the anomaly relation for massive and massless fermion are given in the Appendix.A.

VII. BOGOLIUBOV TRANSFORMATION AND SCHWINGER PAIR PRODUCTION

In order to view the relation of vacuum expectation values and Schwinger pair-productions, we introduce the instantaneous mode[51]. The expansion coefficients of the instantaneous mode are equivalent to Bogoliubov coefficients which diagonalize the Hamiltonian operator $\hat{\mathcal{H}}(t)$ at an arbitrary time t. The time-Bogoliubov coefficients are interpreted as the momentum distribution of pair-created particles at an arbitrary time.

Due to a time-dependent electric field, the momentum and energy of the particles change with time. The original spinor $\phi_{n,n_z}(t)$ is not suitable to describe pair-productions by an applied electric field since they are expanded by the initial energy eigenvectors. Expanding the original spinor $\phi_{n,n_z}(t)$ by the basis that moves with the time-dependent electric field (instantaneous mode), it is possible to describe vacuum expectation values by using the momentum distribution of pair-created particles.

First, we consider a linear transformation for the two-component spinors. The eigenvalues of the time-dependent Hamiltonian for the two-component spinors $\boldsymbol{h}_{n,n_z}(t)\cdot\boldsymbol{\sigma}$ are given by $\pm\omega_{n,n_z}(t) = \pm\sqrt{m^2+2eBn+(k_z-eA(t))^2}$, called the instantaneous energy.

The corresponding eigenvectors are given by

$$\chi^{(+)}_{n,n_z}(t) = \mathrm{e}^{-i\int dt'\omega_{n,n_z}(t')} \begin{pmatrix} \cos(\rho(t)/2) \\ -\sin(\rho(t)/2) \end{pmatrix}, \tag{81}$$

$$\chi^{(-)}_{n,n_z}(t) = \mathrm{e}^{+i\int dt'\omega_{n,n_z}(t')} \begin{pmatrix} \sin(\rho(t)/2) \\ \cos(\rho(t)/2) \end{pmatrix}, \tag{82}$$

where satisfy the eigenvalue equation, $\boldsymbol{h}_{n,n_z}(t)\cdot\boldsymbol{\sigma}\chi^{(\pm)}_{n,n_z}(t) = \pm\omega_{n,n_z}(t)\chi^{(\pm)}_{n,n_z}(t)$, and the angle is given by $\rho(t) = \arctan\Big(\frac{k_z - eA(t)}{\sqrt{m^2+2eBn}}\Big)$, and the global phase factor is called dynamical phase. The eigenvectors coincide with the orthonormal plane wave solutions in $t \to -\infty$, Eqs.(32) and (33).

Note that the instantaneous modes themselves do not satisfy the two-component equation (30). These instantaneous modes satisfy $\chi^{(-)}_{n,n_z} = \Theta\chi^{(+)}_{n,n_z}, \chi^{(+)}_{n,n_z} = -\Theta\chi^{(-)}_{n,n_z}$ and the orthonormal relation $\chi^{\dagger(\pm)}_{n,n_z}\chi^{(\pm)}_{n,n_z} = 1, \chi^{\dagger(\mp)}_{n,n_z}\chi^{(\pm)}_{n,n_z} = 0$.

The time-dependent two-spinor $\phi^{(\pm)}_{n,n_z}(t)$ can be expanded by the instantaneous modes as below,

$$\begin{aligned} \phi^{(+)}_{n,n_z}(t) &= \alpha_{n,n_z}(t)\chi^{(+)}_{n,n_z}(t) + \beta_{n,n_z}(t)\chi^{(-)}_{n,n_z}(t), \\ \phi^{(-)}_{n,n_z}(t) &= -\beta^*_{n,n_z}(t)\chi^{(+)}_{n,n_z}(t) + \alpha^*_{n,n_z}(t)\chi^{(-)}_{n,n_z}(t). \end{aligned} \tag{83}$$

The time-dependent expansion coefficients $\alpha_{n,n_z}(t)$ and $\beta_{n,n_z}(t)$ have information about the non-trivial motion of the spinor $\phi_{n,n_z}(t)$ by an external electric field. Using the orthonormal relation of $\chi^{(\pm)}_{n,n_z}(t)$ and the normalization condition for $\phi^{(\pm)}_{n,n_z}(t)$, (35), one can prove that the time-dependent coefficients $\alpha_{n,n_z}(t), \beta_{n,n_z}(t)$ satisfy the orthonormal condition, $|\alpha_{n,n_z}(t)|^2 + |\beta_{n,n_z}(t)|^2 = 1$, for an arbitrary time t, which is the property of fermionic Bogoliubov coefficients. In the infinite past limit, $t \to -\infty$, the Bogoliubov coefficients become $\alpha_{n,n_z} = 1, \beta_{n,n_z} = 0$ because the initial conditions for two-spinor, Eqs.(32) and (33). In the context of two-level systems, the coefficients, $\alpha_{n,n_z}(t), \beta_{n,n_z}(t)$, mean the ground state population rate and the excited state population rate at each time, respectively.

The relation (83) are equivalent to the realation of mode-functions (four-spinors),

$$\begin{aligned} \psi^{(+,\sigma)}_{\boldsymbol{n}}(t,\boldsymbol{x}) &= \alpha_{n,n_z}(t)\Psi^{(+,\sigma)}_{\boldsymbol{n}}(t,\boldsymbol{x}) + \beta_{n,n_z}(t)\Psi^{(-,-\sigma)}_{\boldsymbol{n}}(t,\boldsymbol{x}) \\ \psi^{(-,-\sigma)}_{\boldsymbol{n}}(t,\boldsymbol{x}) &= -\beta^*_{n,n_z}(t)\Psi^{(+,\sigma)}_{\boldsymbol{n}}(t,\boldsymbol{x}) + \alpha^*_{n,n_z}(t)\Psi^{(-,-\sigma)}_{\boldsymbol{n}}(t,\boldsymbol{x}) \end{aligned} \tag{84}$$

where $\Psi_{\boldsymbol{n}}^{(\pm,\sigma)}(t,\boldsymbol{x})$ are the instantaneous mode-functions, which can be obtained by the replacement $\phi_{n,n_z}^{(\pm)} \to \chi_{n,n_z}^{(\pm)}$ for mode-functions (39)-(42) and satisfy the eigenvalue equation $\hat{H}_D \Psi_{\boldsymbol{n}}^{(\pm,\sigma)}(t,\boldsymbol{x}) = \pm\omega_{n,n_z}(t)\Psi_{\boldsymbol{n}}^{(\pm,\sigma)}(t,\boldsymbol{x})$. The fermionic field operator is expanded by the instantaneous mode-functions,

$$\hat{\psi}(x) = \sum_{n=0}^{\infty}\sum_{n_y=-\mathcal{N}/2}^{\mathcal{N}/2}\sum_{n_z=-\infty}^{\infty}\sum_{\sigma=\uparrow,\downarrow}(\hat{B}_{\sigma,\boldsymbol{n}}(t)\Psi_{\boldsymbol{n}}^{(+,\sigma)}(t,\boldsymbol{x}) + \hat{D}^{\dagger}_{-\sigma,-\boldsymbol{n}}(t)\Psi_{\boldsymbol{n}}^{(-,-\sigma)}(t,\boldsymbol{x})) \tag{85}$$

The time-dependent coefficients, $\hat{B}_{\sigma,\boldsymbol{n}}(t), \hat{D}^{\dagger}_{-\sigma,-\boldsymbol{n}}(t)$, satisfy,

$$\begin{aligned}\hat{B}_{\sigma,\boldsymbol{n}}(t) &= \alpha_{n,n_z}(t)\hat{b}_{\sigma,\boldsymbol{n}} - \beta^{*}_{n,n_z}(t)\hat{d}^{\dagger}_{-\sigma,-\boldsymbol{n}} = U^{\dagger}_{\sigma,\boldsymbol{n}}(t)\hat{b}_{\sigma,\boldsymbol{n}}U_{\sigma,\boldsymbol{n}}(t)\\ \hat{D}^{\dagger}_{-\sigma,-\boldsymbol{n}}(t) &= \beta_{n,n_z}(t)\hat{b}_{\sigma,\boldsymbol{n}} + \alpha^{*}_{n,n_z}(t)\hat{d}^{\dagger}_{-\sigma,-\boldsymbol{n}} = U^{\dagger}_{\sigma,\boldsymbol{n}}(t)\hat{d}^{\dagger}_{\sigma,\boldsymbol{n}}U_{\sigma,\boldsymbol{n}}(t)\end{aligned} \tag{86}$$

where $U_{\sigma,\boldsymbol{n}}(t)$ is the time-dependent unitary operator for each mode defined by the spin-matrix-like operator (56),

$$\begin{aligned}U_{\sigma,\boldsymbol{n}}(t) = &\exp\left(-\frac{i}{2}(-\arg(\alpha_{n,n_z}) + \arg(\beta_{n,n_z}))\tau^3_{\sigma,\boldsymbol{n}}\right)\\ &\times\exp\left(-i\arctan\left(\frac{|\beta_{n,n_z}|}{|\alpha_{n,n_z}|}\right)\tau^2_{\sigma,\boldsymbol{n}}\right)\\ &\times\exp\left(-\frac{i}{2}(-\arg(\alpha_{n,n_z}) - \arg(\beta_{n,n_z}))\tau^3_{\sigma,\boldsymbol{n}}\right).\end{aligned} \tag{87}$$

The relation (86) is a canonical transformation; the anti-commutation relation (48) also holds for the time-dependent annihilation operators, $\hat{B}_{\sigma,\boldsymbol{n}}(t), \hat{D}^{\dagger}_{-\sigma,-\boldsymbol{n}}(t)$.

Using the field operator expanded by the instantaneous mode-functions (85), the Hamiltonian can be easily rewritten,

$$\hat{\mathcal{H}}(t) = \frac{1}{V}\sum_{\sigma=\uparrow,\downarrow}\sum_{n=0}^{\infty}\sum_{n_y=-\mathcal{N}/2}^{\mathcal{N}/2}\sum_{n_z=-\infty}^{\infty}\omega_{n,n_z}(t)(\hat{B}^{\dagger}_{\sigma,\boldsymbol{n}}\hat{B}_{\sigma,\boldsymbol{n}} + \hat{D}^{\dagger}_{-\sigma,-\boldsymbol{n}}\hat{D}_{-\sigma,-\boldsymbol{n}} - 1) \tag{88}$$

$$= \frac{1}{V}\sum_{\sigma=\uparrow,\downarrow}\sum_{n=0}^{\infty}\sum_{n_y=-\mathcal{N}/2}^{\mathcal{N}/2}\sum_{n_z=-\infty}^{\infty}\omega_{n,n_z}(t)U^{\dagger}_{\sigma,\boldsymbol{n}}(t)(\hat{b}^{\dagger}_{\sigma,\boldsymbol{n}}\hat{b}_{\sigma,\boldsymbol{n}} + \hat{d}^{\dagger}_{-\sigma,-\boldsymbol{n}}\hat{d}_{-\sigma,-\boldsymbol{n}} - 1)U_{\sigma,\boldsymbol{n}}(t) \tag{89}$$

So the expectation value of Hamiltonian becomes $\langle F|\,\hat{\mathcal{H}}(t)\,|F\rangle = \langle F'(t)|\,\hat{\mathcal{H}}'(t)\,|F'(t)\rangle$,

where

$$\begin{aligned}\hat{\mathcal{H}}'(t) &= U(t)\hat{\mathcal{H}}(t)U^{\dagger}(t) \\ &= \frac{1}{V}\sum_{\sigma=\uparrow,\downarrow}\sum_{n=0}^{\infty}\sum_{n_y=-\mathcal{N}/2}^{\mathcal{N}/2}\sum_{n_z=-\infty}^{\infty}\omega_{n,n_z}(t)(\hat{b}^{\dagger}_{\sigma,\boldsymbol{n}}\hat{b}_{\sigma,\boldsymbol{n}}+\hat{d}^{\dagger}_{-\sigma,-\boldsymbol{n}}\hat{d}_{-\sigma,-\boldsymbol{n}}-1) \qquad (90)\end{aligned}$$

$$\left|F'(t)\right\rangle = U(t)\left|F\right\rangle = \prod_{\substack{\omega_{n,n_z}>E_F,\\ \sigma=\uparrow,\downarrow}}(\alpha^{*}_{n,n_z}(t)+\beta^{*}_{n,n_z}(t)\hat{d}^{\dagger}_{-\sigma,-\boldsymbol{n}}\hat{b}^{\dagger}_{\sigma,\boldsymbol{n}})\prod_{\substack{\omega_{n,n_z}\leq E_F,\\ \sigma=\uparrow,\downarrow}}\hat{b}^{\dagger}_{\sigma,\boldsymbol{n}}\left|0\right\rangle \qquad (91)$$

$$U(t) = \prod_{\sigma,\boldsymbol{n}}U^{\dagger}_{\sigma,\boldsymbol{n}}(t) \qquad (92)$$

The new Hamiltonian $\hat{\mathcal{H}}'(t)$ is diagonalized, and the new state $|F'(t)\rangle$ describes pair-productions of fermion/antifermion outside the Fermi sphere. It implies that pair-productions do not occur inside the Fermi sphere due to Pauli blocking, and the factor $\beta_{n,n_z}(t)$ has information of pair-created fermion/antifermion for each mode.

The expectation values of Hamiltonian $\langle F|\,\hat{\mathcal{H}}\,|F\rangle$ is described by Bogoliubov coefficients as below,

$$\langle F|\,\hat{\mathcal{H}}\,|F\rangle = \mathcal{H}_{vac}+\mathcal{H}_{f.s.}+\mathcal{H}_{p.p.}, \qquad (93)$$

where

$$\mathcal{H}_{vac} = -\frac{|eB|}{2\pi}\sum_{n=0}^{\infty}\int\frac{\mathrm{d}p_z}{2\pi}\alpha_n\omega_{n,p_z}(t), \qquad (94)$$

$$\mathcal{H}_{f.s.} = \frac{|eB|}{2\pi}\sum_{n=0}^{\infty}\int\frac{\mathrm{d}p_z}{2\pi}\alpha_n\omega_{n,p_z}(t)\theta(p_F^{(n)}-|p_z|), \qquad (95)$$

$$\mathcal{H}_{p.p.} = 2\frac{|eB|}{2\pi}\sum_{n=0}^{\infty}\int\frac{\mathrm{d}p_z}{2\pi}\alpha_n|\beta_{n,p_z}(t)|^2\omega_{n,p_z}(t)\theta(|p_z|-p_F^{(n)}). \qquad (96)$$

When we apply the point-split regularization, the first term $\mathcal{H}_{vac}$ becomes constant, which means the contribution from the vacuum. The second term $\mathcal{H}_{f.s.}$ comes from the Fermi sphere, considering the shift due to an applied electric field. The third term $\mathcal{H}_{p.p.}$ is the contribution from pair-productions outside the Fermi sphere. The factor $|\beta_{n,p_z}|^2$ is interpreted as the momentum distribution of pair-created fermions(antifermions) for the Landau level n. The absence of pair-productions inside the Fermi sphere means the prohibition of pair-productions by Pauli blocking. In the infinite past limit, $t\to-\infty$, the

Bogoliubov coefficients become $\alpha_{n,p_z} = 1, \beta_{n,p_z} = 0$, meaning that no pair-productions occur, so the total energy is

$$\langle F|\,\hat{\mathcal{H}}\,|F\rangle \xrightarrow[t\to-\infty]{} -\frac{|eB|}{2\pi}\sum_{n=0}^{\infty}\int\frac{\mathrm{d}p_z}{2\pi}\alpha_n\omega_{n,p_z} + \frac{|eB|}{2\pi}\sum_{n=0}^{\infty}\int\frac{\mathrm{d}p_z}{2\pi}\alpha_n\omega_{n,p_z}\theta(p_F^{(n)} - |p_z|), \quad (97)$$

which the first term comes from the vacuum and the second term comes from the Fermi sphere.

In the same way, the expectation value of chirality imbalance with the point-split regularization, n_5, is described by Bogoliubov coefficients,

$$n_5 \equiv n_5^{total} = n_5^{f.s} + n_5^{p.p} \quad (98)$$

where

$$n_5^{f.s} = -\frac{eB}{4\pi^2}[\sqrt{m^2 + (p_F - eA(t))^2} - \sqrt{m^2 + (-p_F - eA(t))^2}] \quad (99)$$

$$n_5^{p.p} = \frac{eB}{2\pi}\int\frac{\mathrm{d}p_z}{2\pi}2[-|\beta_{0,p_z}(t)|^2\frac{p_z - eA(t)}{\omega_{0,n_z}(t)} + \frac{m}{\omega_{0,n_z}(t)}\,\mathrm{Re}[\alpha_{0,p_z}(t)\beta^*_{0,p_z}(t)\mathrm{e}^{-2i\int dt'\omega_{0,p_z}(t')}]]\theta(|p_z| - p_F) \quad (100)$$

The first term, $n_5^{f.s}$, comes from the shift of the Fermi sphere. This framework does not consider any scatterings of shifted fermions by an applied electric field, so momentum relaxations do not occur. The second term $n_5^{p.p}$ is interpreted as the contribution from the Schwinger pair production with considering Pauli blocking. The first term of $n_5^{p.p}$ is proportional to the momentum distribution $|\beta_{0,p_z}|^2$ and the relativistic velocity according to z-axis of pair-created fermions, $\frac{p_z - eA(t)}{\omega_{0,n_z}(t)}$. The representation means that chirality imbalance is merely characterized by the momentum(or velocity) distribution of created fermion/antifermion at the lowest Landau level since the spinup-fermions/spindown-antifermions only exist at the lowest Landau level. The second term of $n_5^{p.p}$, which is proportional to $\mathrm{Re}[\alpha_{0,p_z}(t)\beta^*_{0,p_z}(t)\mathrm{e}^{-2i\int dt'\omega_{0,p_z}(t')}]$, can be interpreted as the interference between the non-pair-created and pair-created state for each mode. The term is referred to as polarization current in Ref.[51].

If $E_F = 0$, then $n_5^{f.s} = 0$, that is, the production of chirality imbalance comes from pair-productions by an electric field only. One can find that sufficiently large pair productions are needed to produce chirality imbalance (or electric current). However, sufficiently large

pair productions do not necessarily mean much chirality imbalance (or electric current) because cancellations occur between plus and minus momentum modes. Non-zero chirality imbalance (or electric current) can be obtained if only the momentum distribution is asymmetric, which is discussed in the later section with some specific electric fields.

VIII. AN EVOLUTION OF CHIRALITY IMBALANCE IN ZERO FERMI ENERGY SYSTEM

In this section, we discuss the evolution of chirality imbalance in zero Fermi energy system in a specific electric field by solving equation (30) analytically and numerically.

A. Chirality imbalance in Sauter type electric fields

In this section, we asuume the external electric field as Sauter type one. Assuming this type of electric field, we can obtain the analytical solutions of the Dirac equation, originally proved by Sauter[41]. First, we investigate the evolution of chirality imbalance, electric current and pseudoscalar condensation. Then the vacuum expectation values of chirality imbalance and electric current are relate to the momentum distribution of pair-created particles.

The Sauter type electric field and the corresponding vector potential are given by

$$E(t) = \frac{E}{\cosh^2(t/\tau)}, \tag{101}$$

$$A(t) = -E\tau(\tanh(t/\tau) + 1), \tag{102}$$

where E is the peak of electric field strength and τ is the time-width of electric field. The shape of Sauter type electric field and the corresponding vector potential are shown in Fig.7.

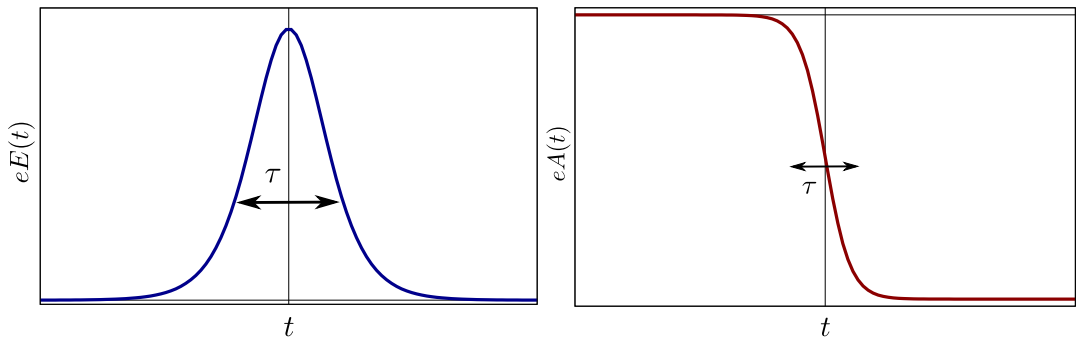

FIG. 7. Time dependence of Sauter type electric field $eE(t)$ and the corresponding vector potential $eA(t)$.

In the Sauter type electric field, the solution of the Dirac equation (30) with the initial condition (32) is given by

$$\phi_{n,k_z}(t) = \begin{pmatrix} \sqrt{\frac{\omega(0)+k_z}{2\omega(0)}} u^{-\frac{i\tau\omega(0)}{2}} (1-u)^{\frac{i\tau\omega(1)}{2}} F\left(\begin{smallmatrix} a,b \\ c \end{smallmatrix}; u(t)\right) \\ \sqrt{\frac{\omega(0)-k_z}{2\omega(0)}} u^{\frac{i\tau\omega(0)}{2}} (1-u)^{-\frac{i\tau\omega(1)}{2}} F\left(\begin{smallmatrix} 1-a,1-b \\ 2-c \end{smallmatrix}; u(t)\right) \end{pmatrix} \tag{103}$$

where $F\left(\begin{smallmatrix} a,b \\ c \end{smallmatrix}; u\right)$ are Gauss's hypergeometric function. The parameters are given by

$$a = 1 - \frac{i\tau\omega_{n,k_z}(0)}{2} + \frac{i\tau\omega_{n,k_z}(1)}{2} + ieE\tau^2 \tag{104}$$

$$b = -\frac{i\tau\omega_{n,k_z}(0)}{2} + \frac{i\tau\omega_{n,k_z}(1)}{2} - ieE\tau^2 \tag{105}$$

$$c = 1 - i\tau\omega_{n,k_z}(0) \tag{106}$$

where

$$\omega^2_{n,k_z}(u(t)) = (k_z + 2eE\tau u(t))^2 + 2|eB|n + m^2 \tag{107}$$

$$u(t) = \frac{1}{2}(\tanh(t/\tau) + 1) \tag{108}$$

Using the analytical solutions of the Dirac equation, we can evaluate the evolution of vacuum expectation values and momentum distribution of pair-created particles by the electric field.

1. An evolution of vacuum expectation values in Sauter type electric fields

We investigate the evolutions of chirality imbalance, electric current and pseudoscalar condensation in Sauter type electric fields. By integrating the integrand at each time according to momentum numerically, we can evaluate the evolution of vacuum expectation values. Here, we have three independent parameters of the model, strength of the electric and magnetic fields, and the fermion mass, which are expressed in units of the electron mass $m_e = 0.5$MeV. We set the cut-off parameter as $\Lambda = 30m_e$, which is much larger than the fermion mass scale.

In our study, we calculate the vacuum expectation values under parallel constant magnetic and the time-dependent Sauter type electric fields, whose strengths can be fixed independently. However, as far as we understand, the chirality imbalance is well studied

by considering the magnetic helicity density h defined in Eq.(80). As we have discussed in the previous section, our calculation is fully consistent to the chiral anomaly relation. In the massless limit, it is simplified as Eq.(79) since we consider the time-independent magnetic field. The integrand of the rhs is just magnetic helicity $h(t)$. Hence, with our electromagnetic field, the chirality imbalance becomes

$$\lim_{t\to\infty} n_5(t) = -\frac{2\alpha}{\pi} \lim_{t\to\infty} h(t) = \frac{e^2 BE\tau}{\pi^2} \tag{109}$$

Nevertheless, it is convenient to express the chirality imbalance (and CME current) in the unit of the magnetic helicity, $e^2 BE\tau/\pi^2$.

In Fig.8, we first show the chirality imbalance n_5 as a function t with a shape of the Sauter electric field by the dash-dotted curve. In the massless case (solid curve), n_5 increases by the electric field, and approaches a finite value, $e^2 BE\tau/\pi^2$, at $t \to \infty$, even after the electric field diminished. On the other hand, in the case of the finite fermion mass, the chirality imbalance consists of both a constant part and an oscillating part at $t \to \infty$. When the mass is comparable with the magnitude of the electric field, $m^2 \sim eE$, the chirality imbalance is largely suppressed as depicted by the dotted curve. Thus, we find that the average chirality imbalance is almost zero, if $m^2 > eE$. We will relate these results with the fermion pair production from the vacuum in view of the Schwinger mechanism [].

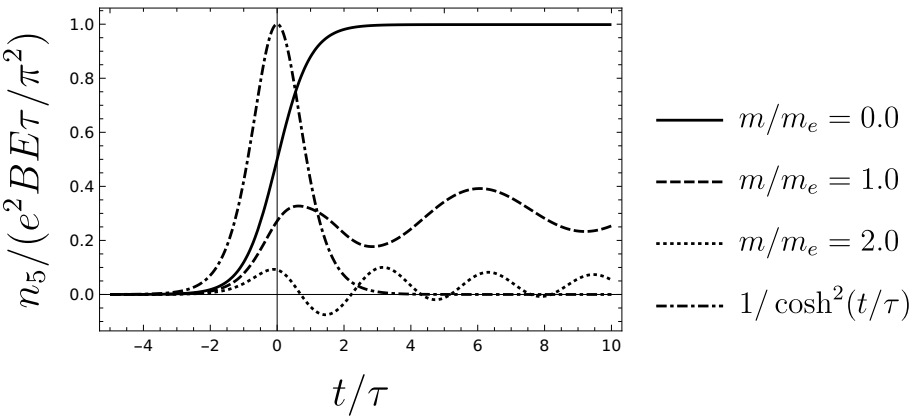

FIG. 8. The time evolution of chirality imbalance n_5. $eE/m_e^2 = 4.0, \tau m_e = 0.5, eB/m_e^2 = 8.0$

We also examine effects of the magnetic field on the chirality imbalance. If we increase the strength of the magnetic field, the magnitude of the chirality imbalance is also increased

which is just proportional to the magnetic helicity. However, the time dependence of n_5 is never changed as expected.

We then show the vector current along the z-direction in Fig.9 which could be understood as the chiral magnetic effect. Again, the vector current is shown in units of the magnetic helicity density. In the case of the massless limit, the vector current depicted by the solid curve consists of a dominant constant part and a tiny oscillating part, which is somewhat different from the behavior of the chirality imbalance n_5. This is because n_5 is solely determined by the lowest Landau level contribution, while the vector current gets contributions from higher Landau levels in Eq.(74) with taking $E_F \to 0$ limit. The average CME current almost vanishes for the small electric field $m^2 > eE$, which is similar with the chirality imbalance.

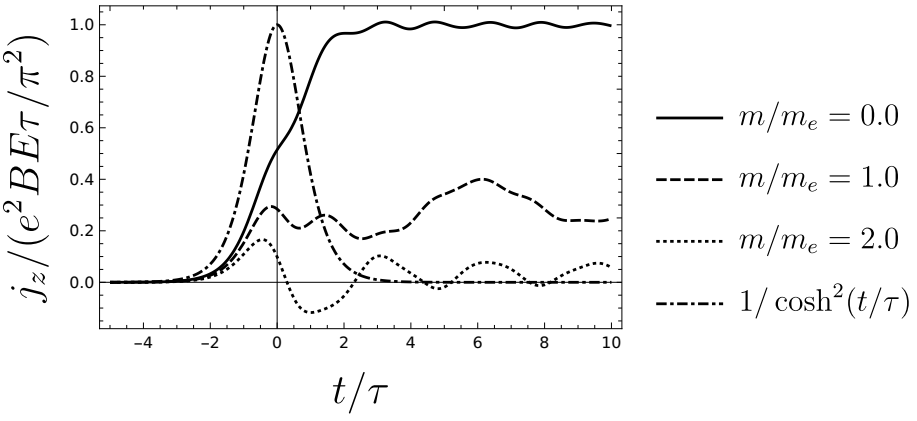

FIG. 9. The time evolution of vector current density j_z. $eE/m_e^2 = 4.0, \tau m_e = 0.5, eB/m_e^2 = 8.0$

From Fig. 9, for $t/\tau \gg 1$ where there is no electric field, the CME current for the massless fermion is expressed as

$$j_z \sim \frac{e^2 BE\tau}{\pi^2} = \frac{\alpha}{2\pi} B(8E\tau) \tag{110}$$

The form of Eq.(110) is the same as Eq.(4) if we substitute $8E\tau$ for μ_5. This crude identification is justified only if t is large enough compared with the timescale τ of the electric field in Eq.(101).

For completeness, we also show the pseudoscalar density in Fig.10 calculated by Eq.(76) with taking $E_F \to 0$ limit. As expected from the chiral anomaly relation Eq.(77), the pseudoscalar density is significant only at $t \sim 0$.

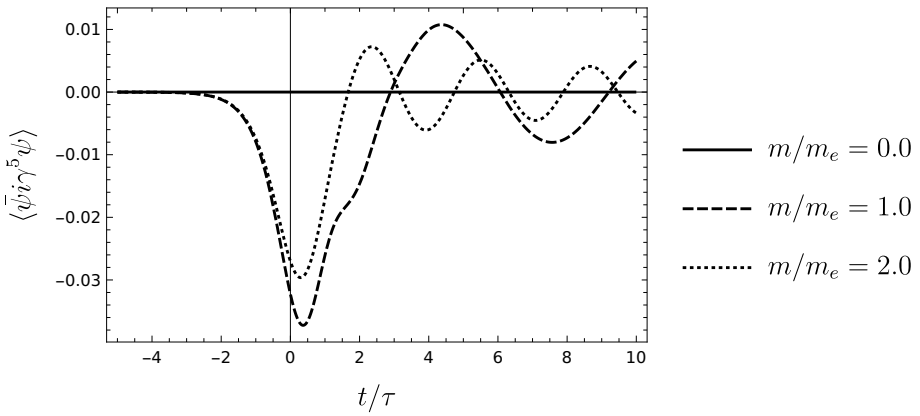

FIG. 10. The time evolution of psuedo-scalar condensate. $eE/m_e^2 = 4.0, \tau m_e = 0.5, eB/m_e^2 = 8.0$

2. Schwinger pair productions in Sauter type electric fields

In order to understand appearance of the chirality imbalance from the vacuum, we relate it with the fermion pair production [51][59][60]. To do so, we try to find a relation between the "in-state" vacuum at $t \to -\infty$ and the "out-state" vacuum at $t \to +\infty$. As discussed in Eqs. (32), (33) and (49), our original in-state vacuum at $t \to -\infty$, $|0\rangle$, coincides with the free particle vacuum (although $B \neq 0$). However, due to the Sauter type electric field, the vacuum at $t \to \infty$, $|0\rangle_{\rm out}$ is not the same as the original vacuum $|0\rangle$.

To proceed calculations, we need asymptotic forms of the mode-function at $t \to -\infty$ and at $t \to \infty$. As mentioned the previous section, the solutions in Sauter type electric fields satisfy the initial conditions for the two-spinor, Eqs. (32) and (33). On the other hand, with the help of the connection formula for the Gauss hypergeometric function, out-state mode-functions are rewritten as

$$\begin{aligned}\phi^{(+)}_{n,n_z}(t) &= \alpha_{n,n_z}\chi^{(+;\rm out)}_{n,n_z}(t) + \beta_{n,n_z}\chi^{(-;\rm out)}_{n,n_z}(t),\\ \phi^{(-)}_{n,n_z}(t) &= -\beta^*_{n,n_z}\chi^{(+;\rm out)}_{n,n_z}(t) + \alpha^*_{n,n_z}\chi^{(-;\rm out)}_{n,n_z}(t).\end{aligned} \tag{111}$$

where out-state two-spinor are given by

$$\chi^{(+;\rm out)}_{n,n_z}(t) = {\rm e}^{-i\omega_{n,k_z}(1)t}\begin{pmatrix}\cos\left(\rho^{\rm out}/2\right)\\ -\sin\left(\rho^{\rm out}/2\right)\end{pmatrix} \tag{112}$$

which are the free fermion wave functions with the energy $\omega(1)$. Here the angle is given by $\rho^{\rm out} = \arctan\left(\frac{k_z+2eE\tau}{\sqrt{m^2+2eBn}}\right)$. In the Sauter type electric field, the Bogoliubov coefficients

are analytically obtained by

$$\alpha_{n,k_z} = \sqrt{\frac{\omega(0)+k_z}{\omega(0)}}\sqrt{\frac{\omega(1)}{\omega(1)+[k_z+2eE\tau]}}\frac{2i}{\tau[\omega(0)+\omega(1)-2eE\tau]} \times \frac{\Gamma(1-i\tau\omega(0))\Gamma(-i\tau\omega(1))}{\Gamma(-\frac{i\tau\omega(0)}{2}-\frac{i\tau\omega(1)}{2}-ieE\tau^2)\Gamma(-\frac{i\tau\omega(0)}{2}-\frac{i\tau\omega(1)}{2}+ieE\tau^2)} \tag{113}$$

$$\beta_{n,k_z} = \sqrt{\frac{\omega(0)+k_z}{\omega(0)}}\sqrt{\frac{\omega(1)}{\omega(1)-[k_z+2eE\tau]}}\frac{2i}{\tau[\omega(0)-\omega(1)-2eE\tau]} \times \frac{\Gamma(1+i\tau\omega(0))\Gamma(-i\tau\omega(1))}{\Gamma(\frac{i\tau\omega(0)}{2}-\frac{i\tau\omega(1)}{2}+ieE\tau^2)\Gamma(\frac{i\tau\omega(0)}{2}-\frac{i\tau\omega(1)}{2}-ieE\tau^2)} \tag{114}$$

From these functions, we can construct the Bogoliubov transformation between in-state and out-state[51][59][60]. We already introduced the annihilation operators and the vacuum for the in-state as in Eq.(49): Similarly, we define the out-state vacuum with operators $\hat{b}^{\rm out}_{\sigma,\boldsymbol{n}}, \hat{d}^{\rm out}_{\sigma,\boldsymbol{n}}$,

$$\hat{b}^{\rm out}_{\sigma,\boldsymbol{n}}|0\rangle = 0,\ \hat{d}^{\rm out}_{\sigma,\boldsymbol{n}}|0\rangle = 0 \text{ (for all } \sigma,\boldsymbol{n}) \tag{115}$$

where operators $\hat{b}^{\rm out}_{\sigma,\boldsymbol{n}}, \hat{d}^{\rm out}_{\sigma,\boldsymbol{n}}$ are introduced as coefficients of $\chi^{(+;{\rm out})}_{n,n_z}(t), \chi^{(-;{\rm out})}_{n,n_z}(t)$ in the same way as time-dependent Bogoliubov coefficients discussed in the section VII. Thus, these operators are subject to the transformation,

$$\begin{aligned}\hat{b}^{\rm out}_{\sigma,\boldsymbol{n}} &= \alpha_{n,n_z}\hat{b}_{\sigma,\boldsymbol{n}} - \beta^*_{n,n_z}\hat{d}^\dagger_{-\sigma,-\boldsymbol{n}} \\ \hat{d}^{\dagger{\rm out}}_{-\sigma,-\boldsymbol{n}} &= \beta_{n,n_z}\hat{b}_{\sigma,\boldsymbol{n}} + \alpha^*_{n,n_z}\hat{d}^\dagger_{-\sigma,-\boldsymbol{n}}\end{aligned} \tag{116}$$

where the Bogoliubov coefficients satisfy the unitary condition $|\alpha_{n,n_z}|^2 + |\beta_{n,n_z}|^2 = 1$ as like the time-dependent ones. The expectation value of the number operator at $t = \infty$ between the original vacuum becomes

$$\langle 0|\,\hat{b}^{\dagger{\rm out}}_{\sigma,\boldsymbol{n}}\hat{b}^{\rm out}_{\sigma,\boldsymbol{n}}|0\rangle = |\beta_{n,n_z}|^2 \tag{117}$$

which is understood as the probability to find a fermion produced by the electric field with the momentum n, k_z at $t = \infty$ [51][59][60]. It is well known that $|\beta_{n,k_z}|^2$ is significant only if the electric field is larger than the fermion mass square, $eE > m^2$, which means spontaneous creation of fermion pairs from the vacuum under the strong electric field. Thus, we naively expect the chirality imbalance may emerge for $eE \gg m^2$.

Using these results, one can express the vacuum expectation values at $t = \infty$ in terms of the Bogoliubov coefficients. For example, the chirality imbalance n_5 at $t = \infty$ is calculated as

$$n_5|_{t=\infty} = \frac{eB}{2\pi}\int_{-\Lambda-2eE\tau}^{\Lambda+2eE\tau}\frac{\mathrm{d}p_z}{2\pi}2[-|\beta_{0,p_z}|^2\frac{p_z+2eE\tau}{\omega_{0,n_z}(1)} + \frac{m}{\omega_{0,n_z}(1)}\,\mathrm{Re}[\alpha_{0,p_z}\beta^*_{0,p_z}\mathrm{e}^{-2i\omega_{0,p_z}(1)t}]] \tag{118}$$

The first term is independent of time, and simply proportional to $|\beta_{0,p_z}|^2$ which is the probability to find a produced particle in the lowest Landau level with k_z. On the other hand, the second term is proportional to the mass and time-dependent, which is interpreted as the "interference" term .

At first sight, n_5 is simply determined by the magnitude of $|\beta_{0,k_z}|^2$. However, existence of the chirality imbalance strongly depends on details of the integration over k_z in Eq. (118), which is sensitive to a parameter τ, the timescale of the electric field in Eq.(101). We will discuss how the nonzero n_5 appears in some detail. In the massless limit, the first term of Eq. (118), which we call $n_5^{(0)}$, becomes

$$n_5^{(0)} = -2\frac{eB}{2\pi}\int_{-\Lambda-2eE\tau}^{\Lambda+2eE\tau}\frac{\mathrm{d}p_z}{2\pi}|\beta_{0,p_z}|^2\frac{p_z+2eE\tau}{\omega_{0,n_z}(1)} \tag{119}$$

$$\xrightarrow[m\to 0]{} -2\int_{-\Lambda-2eE\tau}^{\Lambda+2eE\tau}\frac{\mathrm{d}p_z}{2\pi}\mathrm{sgn}[p_z+2eE\tau]|\beta_{0,p_z}|^2. \tag{120}$$

In the presence of the uniform magnetic field, all the fermions move along the z-direction, and the spin of the fermions in the lowest Landau level, which can contribute to $|\beta_{0,k_z}|$, is parallel to the z-direction. Hence, the fermions with positive mechanical momenta, $pz + 2eE\tau > 0$, carry the right-handed chirality, while those with $pz + 2eE\tau < 0$ are left handed. If the electric field were zero, the imbalance $n_5^{(0)}$ would vanish, because of a cancellation between contributions from $k_z > 0$ and $k_z < 0$ fermions by virtue of the symmetrical k_z distribution of the pair-production probability β_{0,k_z}. However, the nonzero electric field induces an asymmetry between momentum distributions of right- and left-handed fermions in both the sign function $\mathrm{sgn}[k_z + 2eE\tau]$ and the regularization factor $\pm(\Lambda + 2eE\tau)$, which indeed generates the chirality imbalance in this model.

To study $n_5^{(0)}$ in the case of the finite mass, we show $|\beta_{0,k_z}|^2$ and $(k_z + 2eE\tau)/\omega(1)$ in Fig.11, where $(k_z+2eE\tau)/\omega(1)$ is no longer the sign function. The pair-creation probability

$|\beta_{0,k_z}|^2$ peaked at $k_z = -eE\tau$, whereas $(k_z + 2eE\tau)/\omega(1)$ changes its sign at $k_z = -2eE\tau$. Hence, if τ is very small (~ 0), the integration over k_z is negligible due to a cancellation, and thus the resulting chirality imbalance almost vanishes.

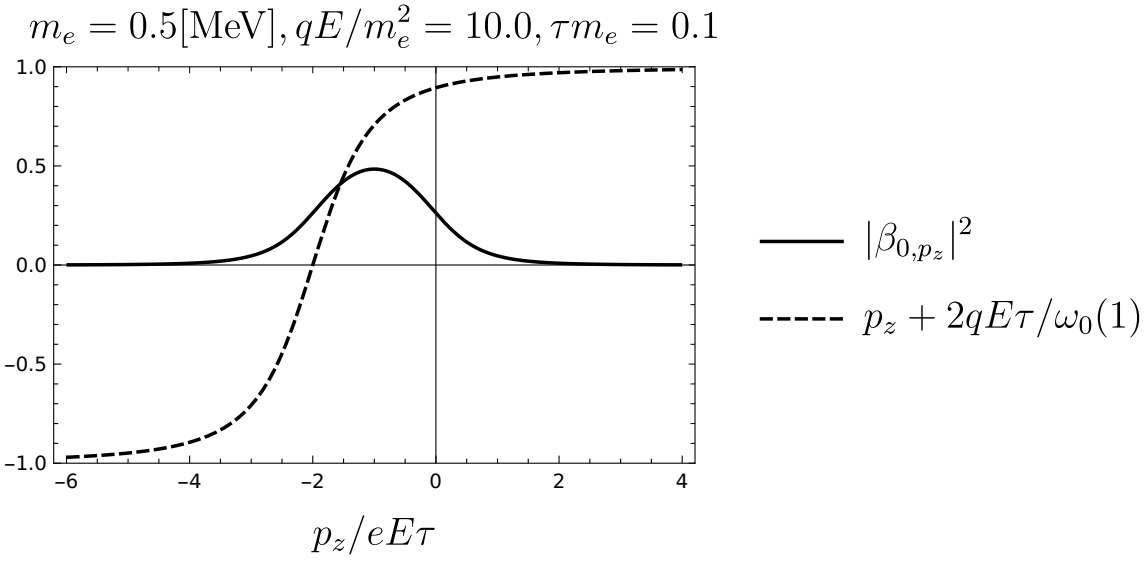

FIG. 11. The plot of the integrand of $\tilde{n}_5$. The chirality of fermions are determined by the sign of $(k_z + 2eE\tau)/\omega(1)$. If fermions are massless, the function become step function. The factor $|\beta_{0,k_z}|^2$ is the momentum distribution of pair producted particles in the lowest Landau level.

For completeness, we show explicit τ dependence of the results. We first show the chirality imbalance as a function of τm_e in Fig.12 for several values of eE. If $eE < m^2$, the chirality imbalance is almost zero, because the production of the fermion pairs is forbidden. The large electric field simply gives the larger chirality imbalance. However, if the timescale τ is quite small, $\tau \ll 1/m_e$, the situation becomes different. In Fig.13, we show $n_5^{(0)}$ for several values of τm_e. We find that, even if the strength of the electric field is large enough, $n_5^{(0)}$ is very small for $\tau m_e < 0.01$. This is because the small τ cannot provide enough asymmetry in the integrand of Eq. (120).

A similar argument holds for the chiral magnetic effect, the z-component of vector

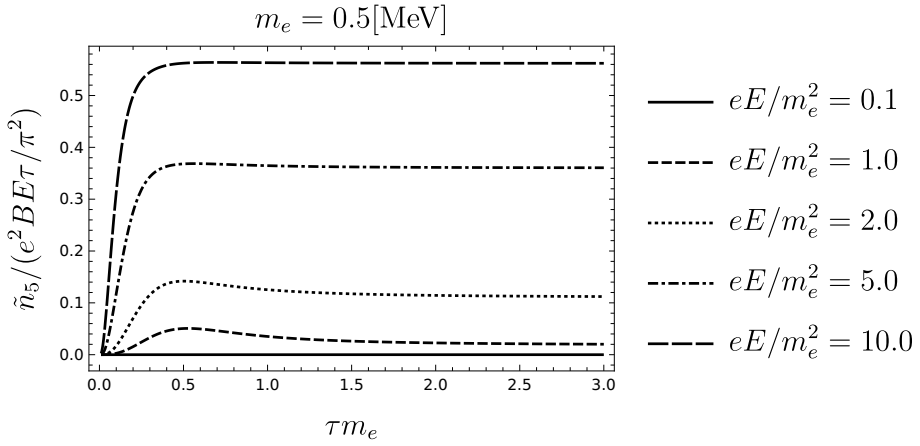

FIG. 12. τ dependence of $n_5^{(0)}$ for several values of eE.

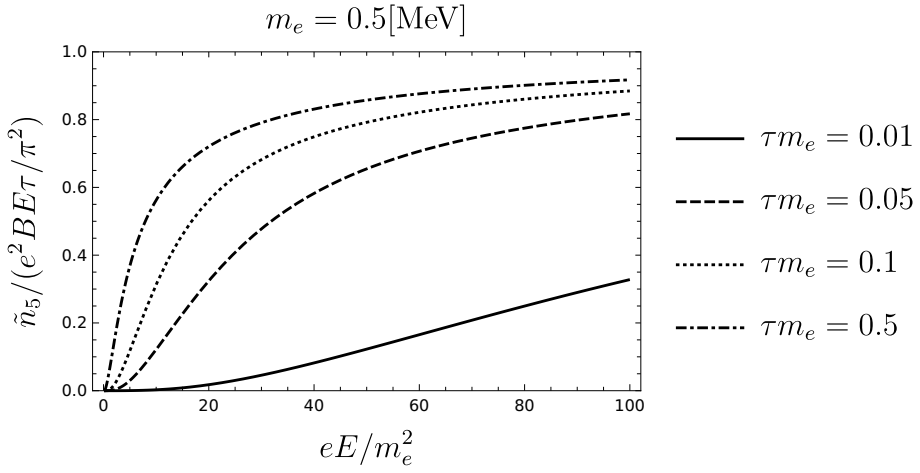

FIG. 13. eE dependence of $n_5^{(0)}$.

current at $t = \infty$. We can write the CME current in terms of Bogoliubov coefficients

$$j_3|_{t=\infty} = \frac{|eB|}{2\pi} \int_{-\Lambda-2eE\tau}^{\Lambda+2eE\tau} \frac{\mathrm{d}p_z}{2\pi} \sum_{n=0}^{\infty} \alpha_n 2[-|\beta_{n,p_z}|^2 \frac{p_z + 2eE\tau}{\omega_{n,n_z}(1)} + \frac{m}{\omega_{n,n_z}(1)} \mathrm{Re}[\alpha_{n,p_z}\beta^*_{n,p_z} \mathrm{e}^{-2i\omega_{n,p_z}(1)t}]] \tag{121}$$

which is similar with one of the chirality imbalance. The first term is independent of time and essentially given by a product of $|\beta_{0,k_z}|^2$ and $(k_z + 2eE\tau)/\omega(1)$, which is interpreted as the z-component of relativistic velocity of particles. Hence, this term is understood as a classical analog of the electric current of the z-component carried by the produced fermions. Note that the second oscillating term is nonzero even in the massless limit.

B. Chirality imbalance in a smooth box type electric field

The evolutions of vacuum expectation values can be evaluated even in an electric field with arbitrary time-dependence by numerically solving the Dirac equation (30). For simplicity of the physical discussion and numerical handling, we assume the time-dependence of electric field, $E(t)$ as smooth-box type. Smooth box type electric field and the corrensponding vector potential satisfied the initial condition (9) are given by

$$E(t) = E(\tanh((t+T/2)/\tau) - \tanh((t-T/2)/\tau))/2 \tag{122}$$

$$A(t) = -E\tau[\log(\cosh((t+T/2)/\tau)) - \log(\cosh((t-T/2)/\tau)) + T/\tau]/2 \tag{123}$$

where E is the strength of electric field, T is the time range over which the electric field and τ is the time interval until the electric field reaches steady state. The time-dependence of the electric field and vector potential are shown by Fig.14. If the solutions of (30) are obtained numerically, then the Bogoliubov coefficients can be easily obtained by using the relation (83), so one can calculate evolutions of chirality imbalance in the finite Fermi energy system and the momentum distribution of pair-created particles at each time.

In this study, we focus on chirality imbalance for massless/massive fermions in the vacuum and massless/massive fermions in finite Fermi energy system. In each case, we calculate the evolution of chirality imbalance and the anomaly relation, and the momentum distribution of pair-producted particles at specific times.

For convenience, the all physical parameters are non-dimensionalized by electron mass, m_e, but the following discussion holds for any energy scale. In the following discussion, we set $m/m_e = 0,1$ as fermion mass, $p_F/m_e = 0,20$ as Fermi momentum and $E/m_e^2 = 2.0, \tau m_e = 0.5, Tm_e = 20.0$ as the parameters of smooth-box type electric field. The strength, E, and time-range, T, are choosen to occur sufficient shift of Fermi sphere and pair-production for massive fermions. The time-interval, τ, is chosen to become closely box-type electric field.

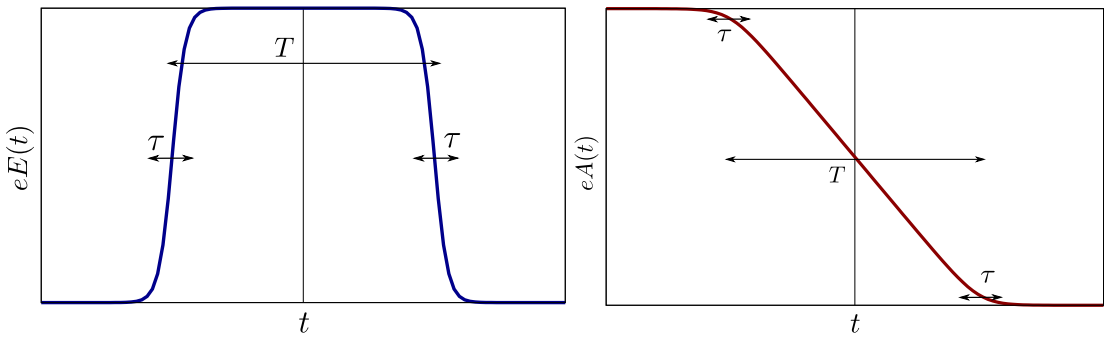

FIG. 14. Time dependence of smooth box type electric field $eE(t)$ and the corresponding vector potential $eA(t)$.

1. *massless fermion in zero Fermi energy system*

First of all, we investigate the evolution of chirality imbalance of massless fermions ($m/m_e = 0$) in the system which the Fermi energy is eqaul to zero, $E_F/m_e = 0$. In massless case, however, the evolution of chirality imbalance is almost trivial since the time-integrated anomaly relation of massless fermion,

$$n_5 = -(e^2/2\pi^2)BA(t). \tag{124}$$

should be satisfied. This simplest case will help in the discussion of the case of massive fermions or/and finite Fermi energy system.

In Fig.15, the evolution of chirality imbalance of massless fermions in the smooth-box type electric field ($E/m_e^2 = 2.0, \tau m_e = 0.5, Tm_e = 20.0$) is shown. The evolution of chirality imbalance is completely equal to the applied vector potential. After the electric field vanished (or equivalently the vector potential becomes constant), the production of chirality imbalance stops and the chirality imbalance is kept at a non-zero value, which is equal to $-(e^2/2\pi^2)BA(t)|_{t=\infty}$.

In Fig.16, the evolution of chirality imbalance, n_5, time-integrated pseudoscalar condensation, $\int dt'\eta(t')$, and vector potential, $eA(t)$, are shown. Clearly, the time-integrated anomaly relation of massless fermion (124) is satisfied. The time-integrated pseudoscalar condensation (or pseudoscalar condensation itself) is always zero. In the analogy of precession of magnetic moments in a magnetic field, it corresponds to the fact that precession

does not occur when there is no transverse magnetic field but only a longitudinal magnetic field that changes with time.

Then, in Fig.17, we show the schematic illustration of dispersion relation in Dirac sea picture and the momentum distribution of pair-created massless fermions in the vacuum in the smooth-box type electric field at some specific times, $t = -15, -5, 5, 20$. Before applying an electric field ($t = -15$), as a matter of course, no pair-production occurs and static massless Dirac vacuum is realized (Fig.17-a). Immediately after the electric field is applied ($t = -5$), the spectral shift is caused by the motion of all the fermions occupying the vacuum as they are accelerated by the electric field(Fig.17-b). Fermions with negative initial momentum(or negative canonical momentum) transition to the state of positive momentum and energy, and the holes after they left behave as antifermions. The momentum distribution of pair-producted fermions is always equal to 1, $|\beta_{0,k_z}|^2 = 1$, since the excitation is gapless. While the electric field is applying ($t = 5$), the momentum distribution spreads in the direction of higher mechanical momentum since the pair-producted fermions and antifermions is accelerated by the electric field simultaneously with pair-productions (Fig.17-c). After the electric field turned off ($t = 15$), the spreading momentum distribution (or equivalently spectral shift) stops, that is, the transition and acceleration by the electric field no longer occur (Fig.20-d).

2. massive fermion in zero Fermi energy system

We also investigate the evolution of chirality imbalance of massive fermions ($m/m_e = 1$) in the vacuum ($p_F = 0$) as the same parameters in the massless case. It is expected that under the sufficiently strong electric field, the production of chirality imbalance occurs but the value is suppressed compared to the massless case due to the mass gap.

The evolution of chirality imbalance of massive fermions in the smooth-box type electric field ($E/m_e^2 = 2.0, \tau m_e = 0.5, T m_e = 20.0$) is shown by Fig.18. Immediately after the application of electric field, the production of chirality imbalance occurs as like the massless case. While the electric field is applying, the production of chirality imbalance continues and its rate of change is proportional to the vector potential, or the impulse felt by the charged fermions due to the electric field, $-eA(t) = \int_{-\infty}^{t} dt' eE(t')$, but the rate is smaller

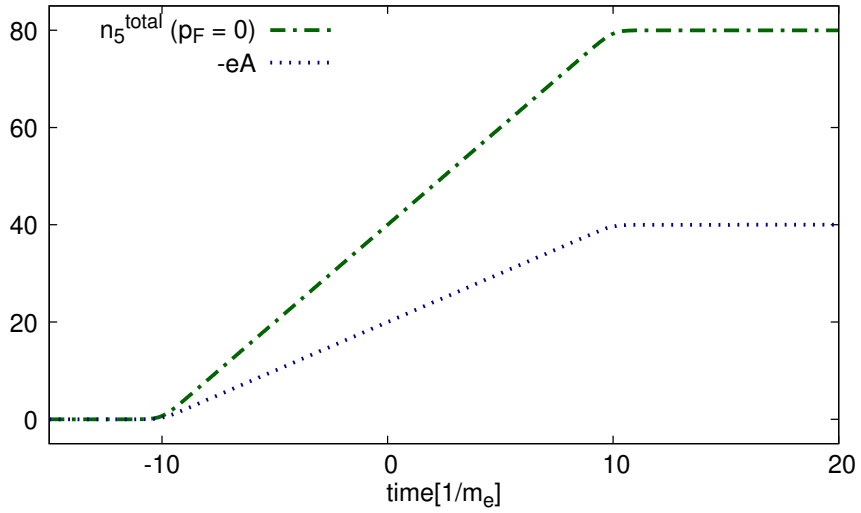

FIG. 15. Time evolution of chirality imbalance for massless fermions in the vacuum ($p_F/m_e = 0.0$) when $E/m_e^2 = 2.0, Tm_e = 20, \tau m_e = 0.5$. The chirality imbalance (dash-dot line) and vector potential (dotted line) are shown. Chirality imbalance are normalized by $eB/4\pi^2$.

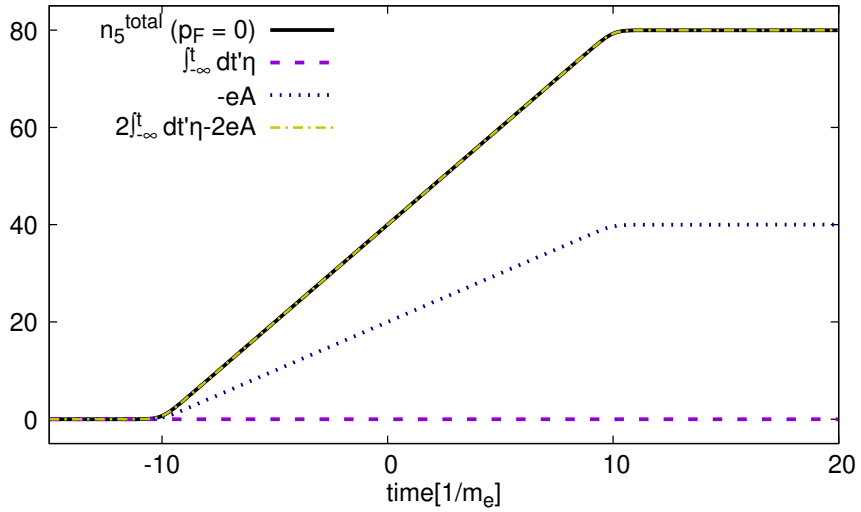

FIG. 16. Time-integrated anomaly relation for massless fermion in the vacuum. Vector potential(dotted line), time-integrated pseudoscalar condensation(dashed line), the sum of these(dash-dot line), and chirality imbalance(solid line) are shown. Chirality imbalance and time-integrated pseudoscalar condensation are normalized by $eB/4\pi^2$. It is shown that time-integrated anomaly relation, $n_5 = 2m\int dt'\eta - (e^2/2\pi^2)BA(t)$, is satisfied.

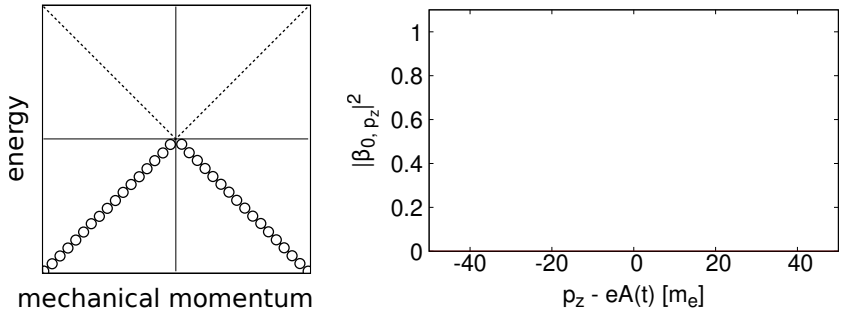

(a) $t = -15$ (before applying the electric field)

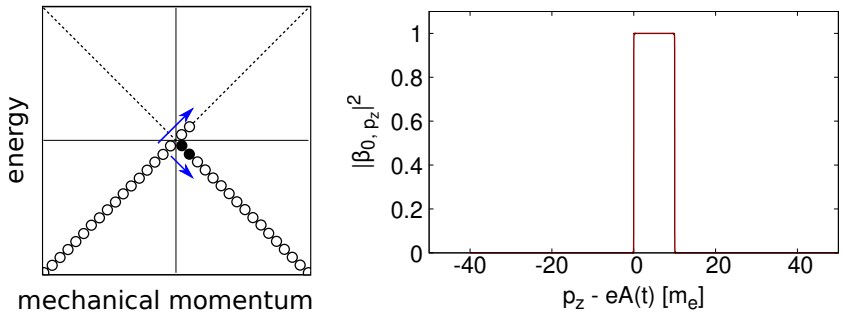

(b) $t = -5$ (immediately after applying the electric field)

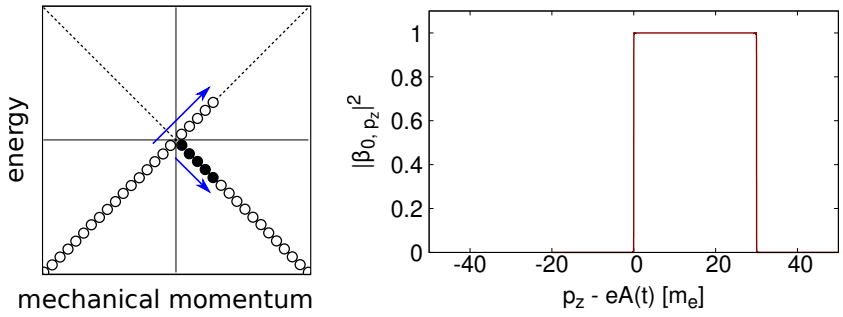

(c) $t = 5$ (after applying the electric field for a while)

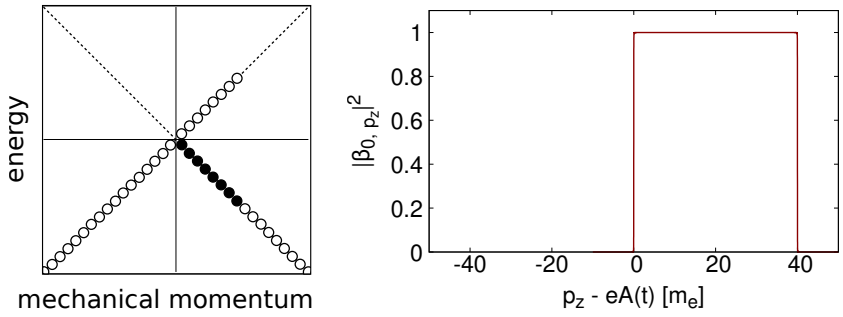

(d) $t = 20$ (after turning off the electric field)

FIG. 17. Schematic illustration of dispersion relation (Dirac sea picuture) and the momentum distribution of pair-created massless fermions in the vacuum at $t = -15, -5, 5, 20$.

than the massless case. After the electric field vanished, the chirality imbalance is kept at non-zero values, but the value is suppressed than the massless one. Unlike the massless case, the oscillation originated from the interference between non-pair-created state and pair-created state is observed.

Then, we investigate how the anomaly relation for massive fermions is satisfied in the smooth-box type electric field. In Fig.19, as like the massless case, chirality imbalance, time-integrated pseudoscalar condensation and vector potential are shown. It is shown that the time-integrated anomaly relation,

$$n_5 = 2m \int_{-\infty}^{t} dt' \eta(t') - \frac{e^2}{2\pi^2} BA(t), \tag{125}$$

is satisfied. The time-integrated pseudoscalar condensation is significantly contributed to the anomaly relation as the fermion mass effect. If the fermions are massless, momentum distribution of pair-producted particles is always equal to 1, $|\beta_{0,k_z}|^2 = 1$, in the range of mechanical momentum, $\Pi_z = [0, -eA(t)]$, because the pair-production is gapless excitation. In the massive case, however, when the strength of electric field is comparable to the fermion mass, the production rate becomes smaller than 1, $|\beta_{0,k_z}|^2 < 1$, since fermions need to cross the mass gap. The time-integrated pseudoscalar condensation compensates for its loss of pair-production, and the anomaly relation holds as a whole.

To see the microscopic behavior of the production of chirality imbalance, the schematic illustration of pair-production and the momentum distribution of pair-created particles at $t = -15, -5, 5, 20$ are shown by Fig.20. As like the massless case, before applying an electric field ($t = -15$), a static vacuum state without pair-productions is realized (Fig.17-a). Immediately after the electric field is applied($t = -5$, Fig.20-b), the pair-production dominantly occur at Dirac point, which is mechanical momentum becomes zero, $\Pi_z(t) = k_z - eA(t) = 0$, or instantaneous energy gap becomes minimum. In the region far from the Dirac point, pair production is strongly suppressed, which is a nature of Schwinger pair-production. While the electric field is applying ($t = 5$, Fig.20-c), pair-production at the Dirac point and acceleration of pair-producted fermions by the electric field occurs, so the momentum distribution spreads in the direction of higher mechanical momentum. The non-zero momentum distribution, $|\beta_{0,k_z}|^2$, exists in the range of mechanical momentum near by $\Pi_z = [0, -eA(t)]$. After the electric field turned off ($t = 15$, Fig.20-d), the

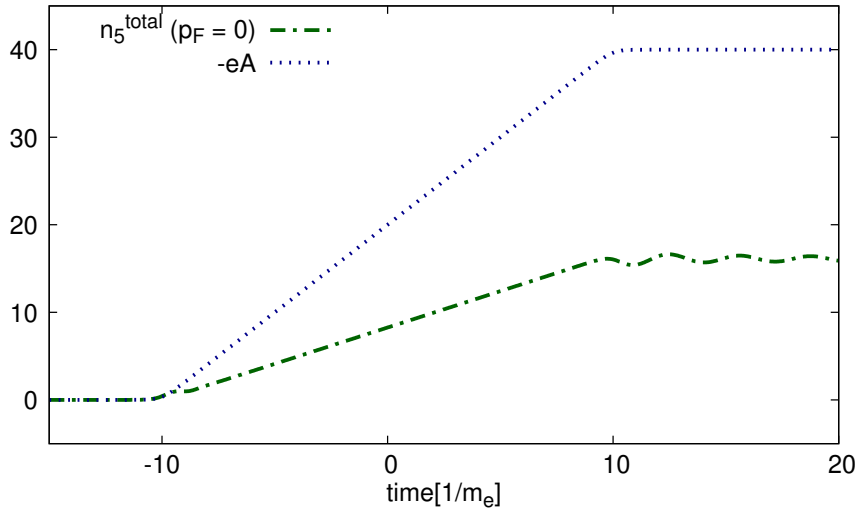

FIG. 18. Evolution of chirality imbalance for massive fermions in the vacuum ($p_F/m_e = 0$) when $E/m_e^2 = 2.0, Tm_e = 20, \tau m_e = 0.5$. The chirality imbalance (dash-dot line) and vector potential (dotted line) are shown.

spreading of the momentum distribution stops as pair production and acceleration by the electric field ceases. Finally, the non-zero pair-production rate dominantly exists in the range of mechanical momentum near by $\Pi_z = [0, -eA(t)|_{t=\infty}]$, and the asymmetry of momentum distribution contributes to the net chirality imbalance.

IX. AN EVOLUTION OF CHIRALITY IMBALANCE IN FINITE FERMI ENERGY SYSTEM

A. massless fermion in finite Fermi energy system

From here on , we consider the case of finite Fermi energy system. We set the Fermi momentum as $p_F = 20.0$ to see both shift of Fermi sphere and pair-production by the applied electric field.

First, the evolution of chirality imbalance of massless fermion ($m/m_e = 0$) is investigated. As like the case of Dirac vaccum, the evolution of chirality imbalance in the smooth-box type electric field ($E/m_e^2 = 2.0, \tau m_e = 0.5, Tm_e = 20.0$) is shown by Fig.21 , which the contribution from shift of Fermi sphere, $n_5^{f.s.}$, and pair-production, $n_5^{p.p.}$, are

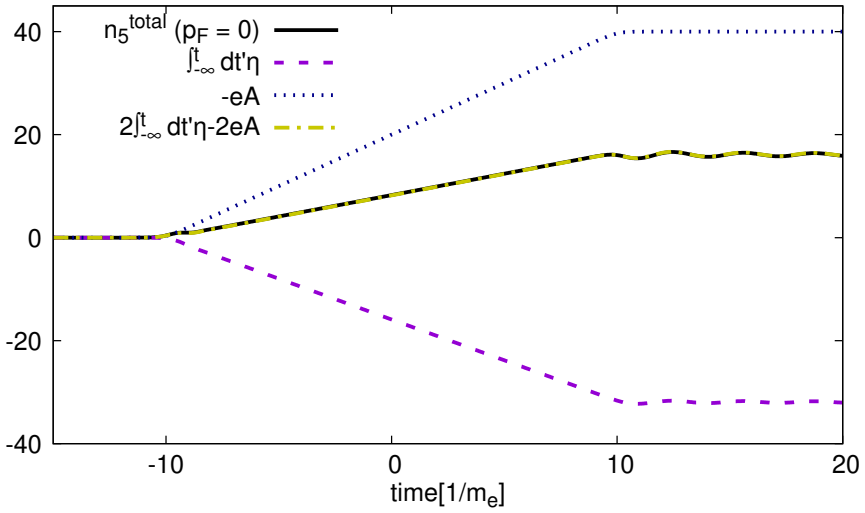

FIG. 19. Time-integrated anomaly relation for massive fermion in the vacuum ($p_F/m_e = 0$). Vector potential (dotted line), time-integrated pseudoscalar condensation (dashed line), the sum of these (dash-dot line), and chirality imbalance (solid line) are shown. Chirality imbalance and time-integrated pseudoscalar condensation are normalized by $eB/4\pi^2$. It is shown that time-integrated anomaly relation, $n_5 = 2m\int dt'\eta - (e^2/2\pi^2)BA(t)$, is satisfied.

shown separately. In fact, the evolution of total chirality imbalance is completely same as the case of the zero Fermi energy system, but the mechanism of evolution of chirality imbalance is different as follows. Immediately after electric field is applied, the production of chirality imbalance occurs as like the vacuum, but the origin is the shift of Fermi sphere, $n_5^{f.s.}$, not pair-production, $n_5^{p.p.}$. At near $t = 0$, which is the time when the vector potential equals the Fermi momentum, the contribution from the shift of Fermi sphere becomes constant, and instead, the contribution from pair-production, $n_5^{p.p.}$, begins to increase. After the electric field vanished, as like the case of the zero Fermi energy system, the production of chirality imbalance stops and the chirality imbalance is kept at a non-zero value, which is equal to $-(e^2/2\pi^2)BA(t)|_{t=\infty}$.,

As the same way, the evolution of chirality imbalance, n_5, time-integrated pseudoscalar condensation, $\int dt'\eta(t')$, and vector potential, $eA(t)$, are shown in Fig.22. The time-integrated anomaly relation of massless fermion (124) is satisfied even in Fermi vaccum.

The schematic illustration of the shift of Fermi sphere and pair-production, and the

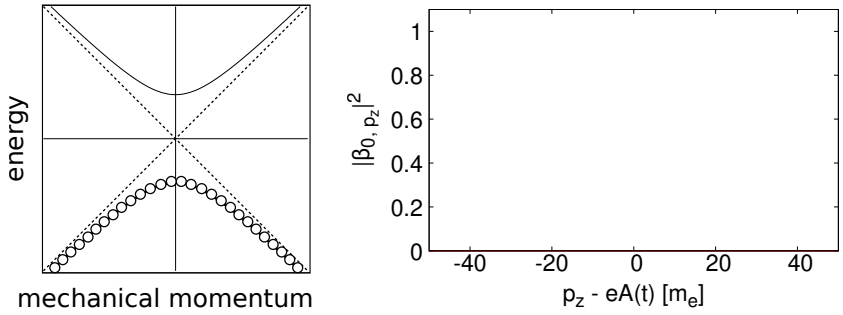

(a) $t = -15$ (before applying the electric field)

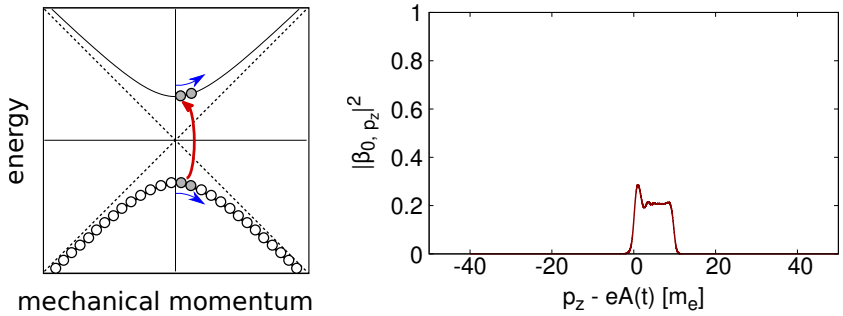

(b) $t = -5$ (immediately after applied the electric field)

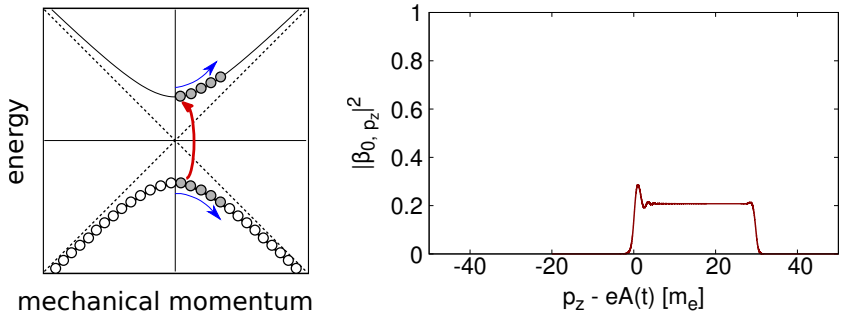

(c) $t = 5$ (after applying the electric field for a while)

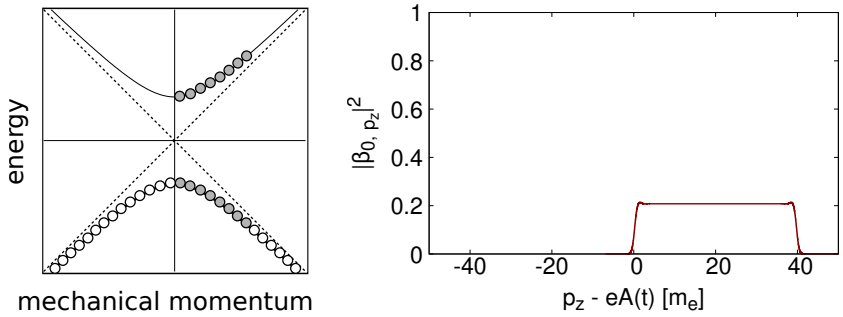

(d) $t = 20$ (after turned off the electric field)

FIG. 20. Schematic illustration of dispersion relation (Dirac sea picuture) and the momentum distribution of pair-created massive fermions in the vacuum at $t = -20, -5, 5, 20$.

momentum distribution of Fermi sphere and pair-producted particles at specific time $t = -15, -5, 5, 20$ are shown by Fig.23. Before the application of the electric field ($t = -15$), the Fermi sphere on the vacuum of massless fermions is realized (Fig.23-a). Chirality imbalance does not exist because the Fermi sphere is symmetric according to momentum. Immediately after the application of the electric field ($t = -5$), all fermions occupied in the vacuum and the Fermi sphere are moved by the applied electric field (Fig.23-b). In this time region, the transition from negative to positive energy does not occur until the Fermi surface reachs the Dirac point ($t = 0$) because fermions are already occupied in positive energy levels. As soon as the Fermi surface go over the Dirac point ($t = 5$), the transition from negative to positive energy start to occur (Fig.23-c). After the electric field turned off ($t = 20$), just like the case of the zero Fermi energy system, the transition and acceleration by the electric field stop, so the shift of Fermi sphere and spreading the momentum distribution also stop(Fig.23-d).

In the massless case, there is no distinction between the vacuum and the finite Fermi energy system in terms of the production of net chirality imbalance. In the case of massive fermions, however, the zero Fermi energy system and the finite Fermi energy one can be distinguished, as will be shown in the next section.

B. massive fermion in finite Fermi energy system

Finally, we investigate the case of massive fermions in finite Fermi energy system. As in previous discussions, we set the Fermi momentum as $p_F/m_e = 20.0$ and the parameter of smooth-box type electric field as $E/m_e^2 = 2.0, \tau m_e = 0.5, Tm_e = 20.0$.

The evolution of chirality imbalance of massive fermions in the smooth-box type electric field is shown by Fig.24, which the contribution from shift of Fermi sphere, $n_5^{f.s.}$, and pair-production, $n_5^{p.p.}$, are shown separately. Immediately after electric field is applied, the production of chirality imbalance occurs, which comes from the shift of Fermi sphere, $n_5^{f.s.}$, not pair-production, $n_5^{p.p.}$, as like the case of massless fermions in finite Fermi energy system. At near $t = 0$, which is the time when the Fermi surface reachs the Dirac point, the contribution from the shift of Fermi sphere becomes constant, and instead, the contribution from pair-production, $n_5^{p.p.}$, begins to increase. Unlike the case of massless

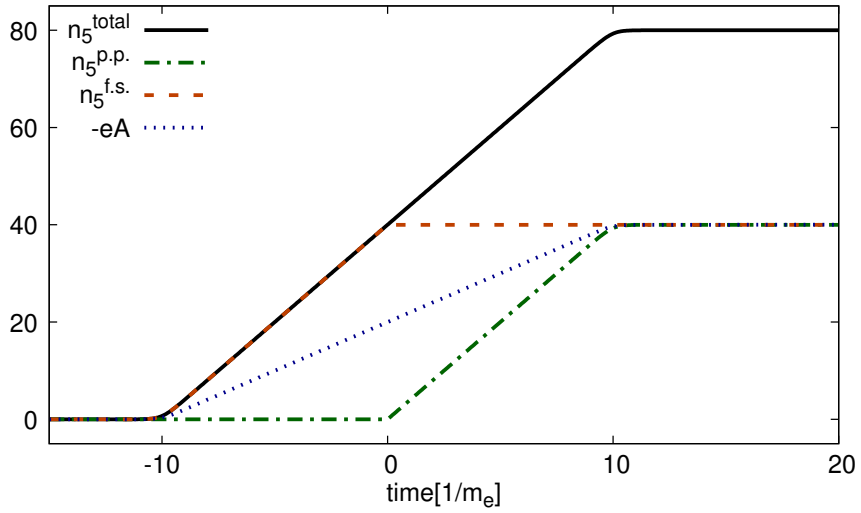

FIG. 21. Evolution of chirality imbalance for massless fermions in the finite Fermi energy system ($p_F = 20.0$). The chirality imbalance produced by the shift of Fermi sphere (dashed line), by pair-production (dash-dot line), the total chirality imbalance (solid line) and vector potential (dotted line) are shown.

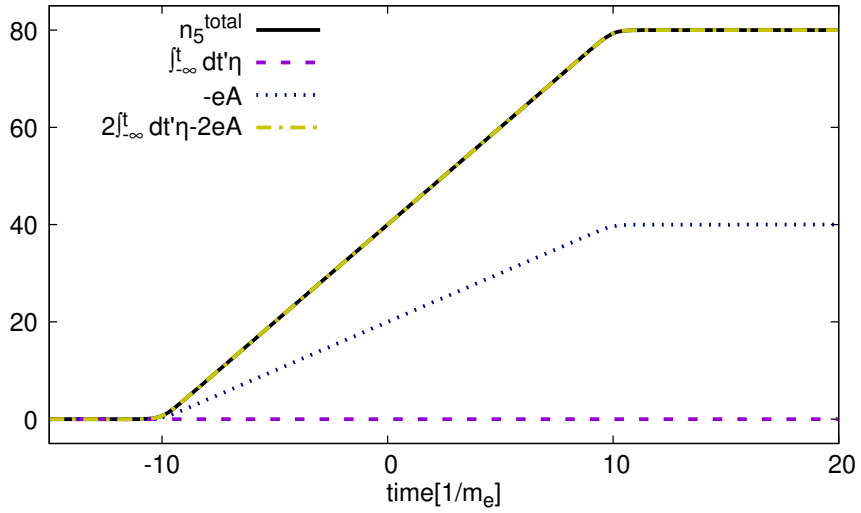

FIG. 22. Time-integrated anomaly relation for massless fermion in the finite Fermi energy system ($p_F/m_e = 20.0$). Vector potential(dotted line), time-integrated pseudoscalar condensation(dashed line), the sum of these(dash-dot line), and chirality imbalance(solid line) are shown. Chirality imbalance and pseudoscalar condensation are normalized by $eB/4\pi^2$. It is shown that time-integrated anomaly relation, $n_5 = -(e^2/2\pi^2)BA(t)$, is satisfied even in finite Fermi energy system.

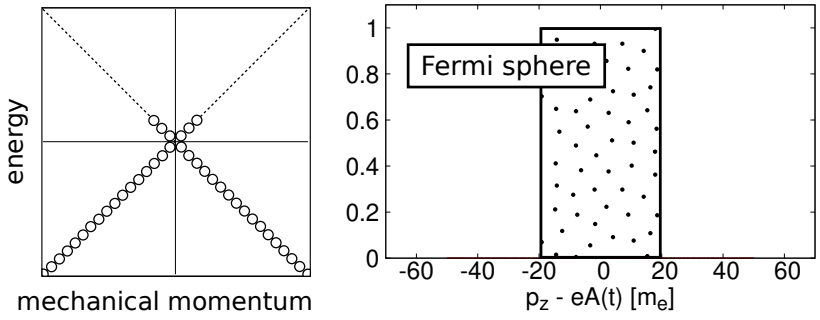

(a) $t = -15$ (before applying the electric field)

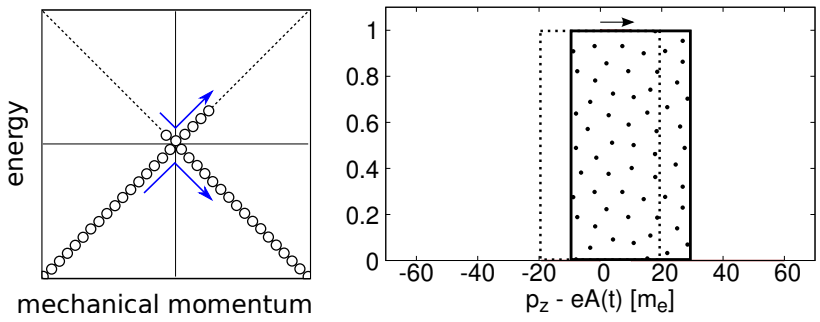

(b) $t = -5$ (immediately after applying the electric field)

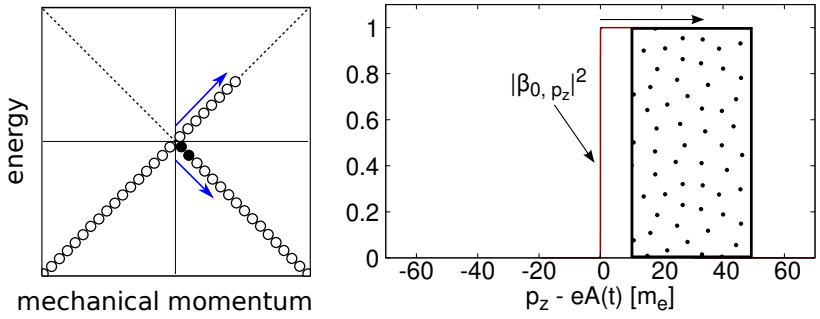

(c) $t = 5$ (after applying the electric field for a while)

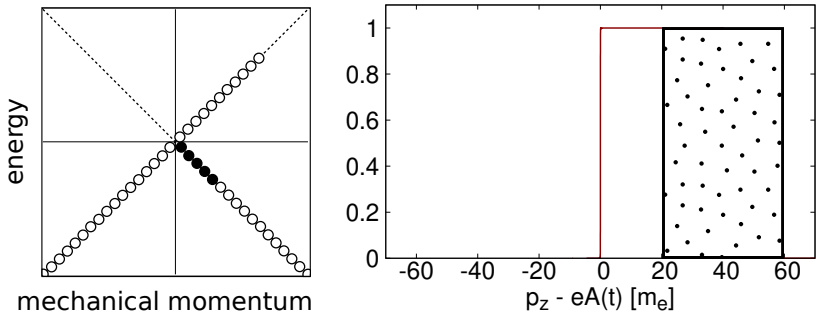

(d) $t = 20$ (after turned off the electric field)

FIG. 23. Schematic illustration of dispersion relation (Dirac sea picuture), and the momentum distribution of Fermi sphere and pair-created massless fermions at $t = -15, -5, 5, 20$

fermions in finite Fermi energy system, the time variation of chirality imbalance becomes more gradual. After the electric field vanished, the production of chirality imbalance stops and the chirality imbalance is kept at a non-zero value and the oscillation came from interference is observed as like the case of massive fermions in the zero Fermi energy system.

The anomaly relation for massive fermoins is satisfied even in finite Fermi energy system, it is shown by Fig.25. The production of time-integrated pseudoscalar condensation occurs after the Fermi surface went over the Dirac point as like the increase of $n_5^{p.p.}$. This implies that the mass effect in the anomaly relation comes only the contribution from pair-productions.

To investigate the microscopic behavior of the evolution of chirality imbalance, we show the schematic illustration of the shift of Fermi sphere and pair-production, and the momentum distribution of Fermi sphere and pair-producted particles in Fig.26. Before the application of the electric field ($t = -15$), the Fermi sphere of massless fermions is realized (Fig.26-a). Chirality imbalance does not exist because the momentum distribution of Fermi sphere is symmetric. Immediately after the application of the electric field ($t = -5$), the shift of Fermi sphere occurs as like finite Fermi energy system. Until $t = 0$, which is the time when Fermi surface reachs the Dirac point (or equivalently vector potential equals the Fermi momentum), pair-productions by the electric field does not occur because of Pauli blocking (Fig.26-b). After the Fermi surface go over the Dirac point ($t = 5$), pair-productions by the electric field start to occur and the pair-producted fermions is accelerated (Fig.26-c). After the electric field turned off, just like the case of the zero Fermi energy system, pair-productions and acceleration by the electric field cease (Fig.26-d).

In massless case, the slope of the time variation of $n_5^{f.s.}$ and $n_5^{p.p.}$ is equal, that is, the total chirality imbalance, n_5^{total}, is completely equal to the vector potential. In the massive case, however, the production of chirality imbalance from the shift of Fermi sphere and pair-production is distinguishable by the slope of the time variation.

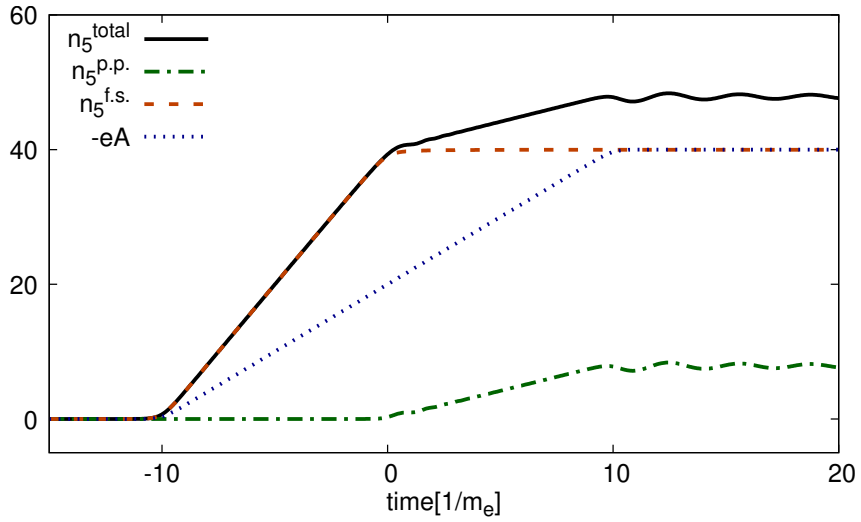

FIG. 24. Evolution of chirality imbalance for massive fermions in finite Fermi energy system ($p_F = 20.0$). The chirality imbalance by the shift of Fermi sphere (dashed line), chirality imbalance by pair-production(dash-dot line), the total chirality imbalance (solid line) and vector potential (dotted line) are shown.

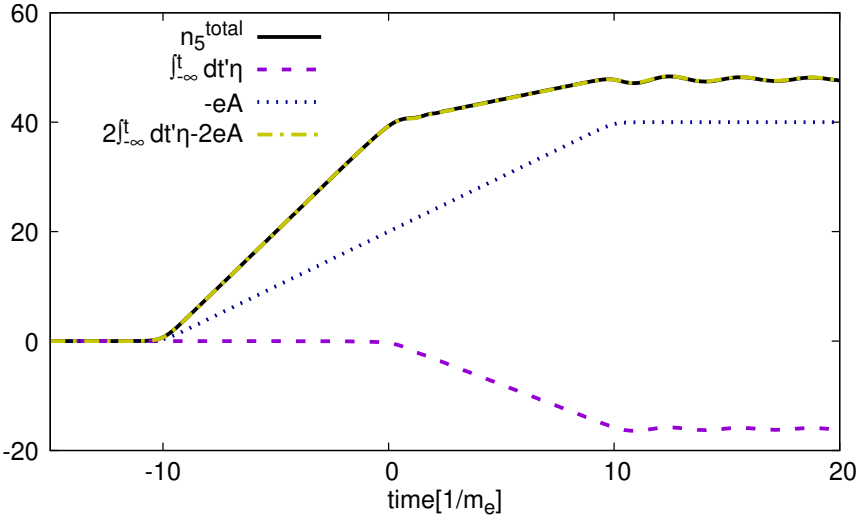

FIG. 25. Time-integrated anomaly relation for massive fermion in the finite Fermi energy system ($p_F/m_e = 20.0$). Vector potential(dotted line), time-integrated pseudoscalar condensation(dashed line), the sum of these(dash-dot line), and chirality imbalance(solid line) are shown. Chirality imbalance and pseudoscalar condensation are normalized by $eB/4\pi^2$. It is shown that time-integrated anomaly relation, $n_5 = 2m\int dt'\eta - (e^2/2\pi^2)BA(t)$, is satisfied even in finite Fermi energy system.

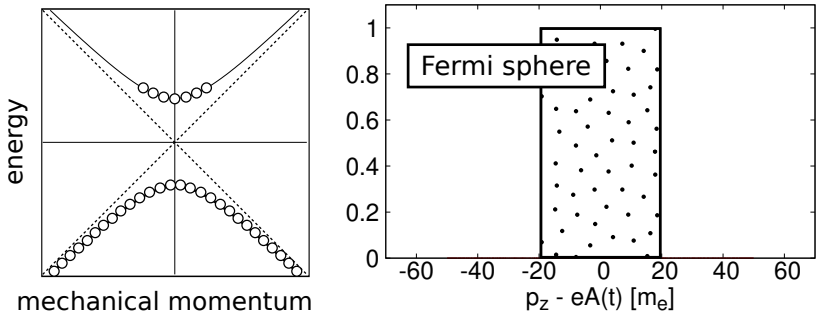

(a) $t = -15$ (before applying the electric field)

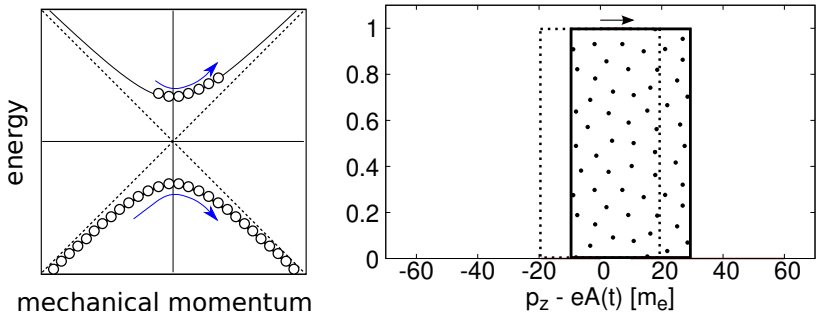

(b) $t = -5$ (before the Fermi surface crosses the Dirac point)

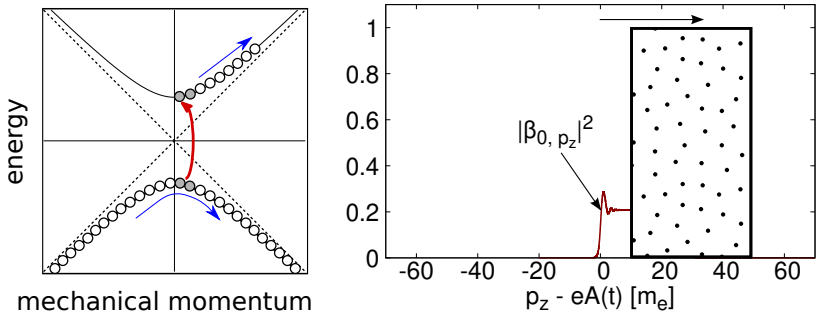

(c) $t = 5$ (after the Fermi surface crosses the Dirac point)

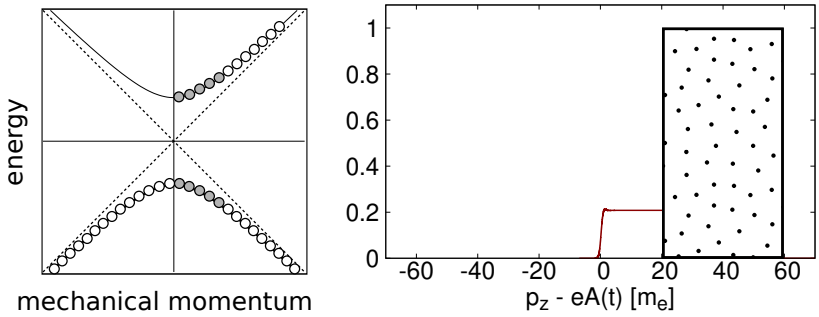

(d) $t = 20$ (after turned off the electric field)

FIG. 26. Schematic illustration of dispersion relation ((Dirac sea picuture)), and the momentum distribution of Fermi sphere and pair-created massive fermions at $t = -15, -5, 5, 20$

X. CONCLUSIONS

Recently, anomalous transport phenomena, such as chiral magnetic effct or chiral separation effect, are investigated by using various theoretical approachs. The relation between chiral anomaly and Schwinger pair-production is also interested. So we investigate vector current and axial-vector current in a parallel electric field and magnetic field with non-zero total particle number by solving the Dirac equation in homogeneous time-dependent electric field and time-independent magnetic field. The fermionic field operator is expanded by the solutions of Dirac equation and the vacuum state and finite Fermi energy system are constructed. The expectation values of vector and axial-vector current are calculated in gauge invariant way by using the point-split regularization. Under a strong magnetic field, chirality imbalance is equal to electric current except the sign, since the production of electric current contributed from higher Landau levels are strongly suppressed. This is the chiral magnetic effect in this framework.

To see the relation between chiral imbalance and Schwinger pair-production, we introduce the instantaneous modes and Bogoliubov coefficients to describe the expectation values by the momentum distribution of pair-created particles. The expectation values of the Hamiltonian can be described separately by Dirac vaccum, Fermi sphere and pair-production contributions taking into accout the acceleration by an applied electric field. It is shown that pair-productions does not occur inside the Fermi sphere due to Pauli blocking.

Chirality imbalance and electric current can be evolved by an applied electric field in the strong electric field. The production of chirality imbalance (or electric current) can be separated into the contribution by the shift of Fermi sphere and pair-production taking into acccount Pauli blocking. We set smooth-box type as the applied electric field and calculate the evolution of chirality imbalance and the momentum distribution of pair-producted fermions by solving the time-dependent part of Dirac equation numerically. In a smooth-box type electric field, immediately after applying the electric field, the shift of Fermi sphere occur and contribute to the net chirality imbalance. The pair-production can occur dominantly only after the Fermi surface went over the Dirac point. Chirality imbalance is kept at non-zero values even after the electric field turned off. If fermions

are massive, the oscillation originated the interference between non-pair-created state and pair-created state is observed. In the massless case, the production of chirality imbalance from the shift of Fermi sphere and pair-production are completely same. In the massive case, however, these are distinguishable by the slope of the time variation.

Chirality imbalance is evolved with satisfying anomaly relation but the evolution of mass term is non-trivial. So we investigate the time-integrated pseudoscalar condensation as fermion mass effect. If the strength of electric field is comparable to the fermion mass, the time-integrated pseudoscalar condensation significantly contribute to the time-integrared anomaly relation since fermions need to cross the mass gap and the production rate is always smaller than the massless case.

In contrary to chirality imbalance and electric current, total number density and spin are time-independent even if any electric fields exist, in other words, these are conserved quantity. If the magnetic field is greater than Fermi momentum, spin expectation value is equal to total number density except the sign. It seems that this is the chiral magnetic effect in this framework but the spin expectation value, s_3, does not appear to be generated by the anomaly effect because the spin expectation value exists even before a electric field applied.

This study is significant in that it clarifies the microscopic and nonequilibrium nature of chiral transport phenomena.

ACKNOWLEDGEMENT

I am grateful to my supervisor Prof. K. Suzuki for many instructive suggestions, valuable discussion, and continuous supports. I would like to express my sincere gratitude to Prof. A. Suzuki, Prof. S. Furusawa, and Prof. J. Usukura for their instructive suggestions and fruitful discussion.

I would like to acknowledge Prof. R. Kase, Dr. S. Nakamura, K. Tamura and F. Terazaki for their kind help. I also thank all the members of the Quark/Hadron Physics Group of Tokyo University of Science.

Appendix A: Anomaly relation

In this section, we will proof the anomaly relation (77). Before discussed the time-derivative of chirality imbalance, we prepare the transformation from the two-component equation to Bloch equation. The two-component equation (30) can be transformed to Bloch equation without relaxation terms as below,

$$\partial_t \boldsymbol{s}_{n,k_z} = 2\boldsymbol{h}_{n,k_z} \times \boldsymbol{s}_{n,k_z} \tag{A1}$$

where $\boldsymbol{s}_{n,k_z}$ is the Bloch's vector and its i-th component is defined by $s^{(i)}_{n,k_z} = \phi^\dagger_{n,k_z}\sigma^i\phi_{n,k_z}$. Note that the continuum limit $k_z = 2\pi n_z/L_z \to k_z$ has been taken. The equation (A1) is explicitly written by

$$\partial_t \begin{pmatrix} s^{(1)}_{n,k_z} \\ s^{(2)}_{n,k_z} \\ s^{(3)}_{n,k_z} \end{pmatrix} = \begin{pmatrix} 0 & -(k_z - eA(t)) & 0 \\ k_z - eA(t) & 0 & -\sqrt{m^2 + 2|eB|n} \\ 0 & \sqrt{m^2 + 2|eB|n} & 0 \end{pmatrix} \begin{pmatrix} s^{(1)}_{n,k_z} \\ s^{(2)}_{n,k_z} \\ s^{(3)}_{n,k_z} \end{pmatrix} \tag{A2}$$

By using the Bloch's vector, the regularized chirality imbalance and pseudoscalar condensation become

$$n_5 = \frac{eB}{2\pi}\int_{-\Lambda+eA(t)}^{\Lambda-eA(t)} \frac{dk_z}{2\pi} s^{(3)}_{0,k_z}(t)\theta(|k_z| - p_F), \tag{A3}$$

$$\eta = \frac{eB}{2\pi}\int_{-\Lambda+eA(t)}^{\Lambda-eA(t)} \frac{dk_z}{2\pi} s^{(2)}_{0,k_z}(t)\theta(|k_z| - p_F). \tag{A4}$$

Next, we consider the time-derivative of regularized chirality imbalance (A3),

$$n_5(t+\Delta t) = \frac{eB}{2\pi}\int_{-\Lambda+eA(t+\Delta t)}^{\Lambda-eA(t+\Delta t)} \frac{dk_z}{2\pi} s^{(3)}_{n,k_z}(t+\Delta t)\theta(|k_z| - p_F) \tag{A5}$$

$$= \frac{eB}{2\pi}\int_{-\Lambda+eA(t)+e\dot{A}(t)\Delta t}^{\Lambda-eA(t)-e\dot{A}(t)\Delta t} \frac{dk_z}{2\pi} [s^{(3)}_{n,k_z}(t) + \dot{s}^{(3)}_{n,k_z}(t)\Delta t]\theta(|k_z| - p_F) \tag{A6}$$

where we use Taylor expansion for $eA(t+\Delta t)$ and $s^{(3)}_{n,k_z}(t+\Delta t)$ in the last equality. By

using (A1) and dividing the integral interval,

$$
\begin{aligned}
n_5(t+\Delta t) = & \frac{eB}{2\pi}\int_{-\Lambda+eA(t)}^{\Lambda-eA(t)} \frac{dk_z}{2\pi}[s^{(3)}_{n,k_z}(t) + 2ms^{(2)}_{n,k_z}(t)\Delta t]\theta(|k_z|-p_F) \\
& + \frac{eB}{2\pi}\int_{\Lambda-eA(t)}^{\Lambda-eA(t)-e\dot{A}(t)\Delta t} \frac{dk_z}{2\pi}[s^{(3)}_{n,k_z}(t) + 2ms^{(2)}_{n,k_z}(t)\Delta t]\theta(|k_z|-p_F) \\
& + \frac{eB}{2\pi}\int_{-\Lambda+eA(t)+e\dot{A}(t)\Delta t}^{-\Lambda+eA(t)} \frac{dk_z}{2\pi}[s^{(3)}_{n,k_z}(t) + 2ms^{(2)}_{n,k_z}(t)\Delta t]\theta(|k_z|-p_F)
\end{aligned}
\tag{A7}
$$

The first term becomes $n_5(t) + 2m\eta(t)\Delta t$, which is corresponding to the classical term. The second and third term are the contribution from the edge of large momentum integral. So we need to know the behavior of the integrand in the ultraviolet region. The initial values of $s^{(3)}_{0,k_z}(t), s^{(2)}_{0,k_z}(t)$ is easily obtained by (32) and (33),

$$
\lim_{t\to-\infty} s^{(3)}_{0,k_z}(t) = \frac{k_z}{m^2+k_z^2} \tag{A8}
$$

$$
\lim_{t\to-\infty} s^{(2)}_{0,k_z}(t) = 0 \tag{A9}
$$

This is the relativestic velocity of fermions in the lowest Landau level. This implies that the integrand in the ultraviolet region becomes

$$
\lim_{k_z\to\pm\infty} s^{(3)}_{0,k_z}(t) \to \pm 1, \quad \lim_{k_z\to\pm\infty} s^{(2)}_{0,k_z}(t) \to 0 \tag{A10}
$$

for an arbitrary time since the modes in the ultraviolet region are hardly affected by an applied electric field. By taking the momentum cut-off, which is sufficiently larger than the Fermi momentum and the parameters of electric field such as typical time-scale and strength, the contribution from the edge of large momentum integral becomes

$$
\begin{aligned}
n_5(t+\Delta t) = & \, n_5(t) + 2m\eta(t)\Delta t \\
& + \frac{eB}{4\pi^2}(-e\dot{A}(t)\Delta t)(+1) + \frac{eB}{4\pi}e\dot{A}(t)\Delta t)(-1)
\end{aligned}
\tag{A11}
$$

So we can obtain

$$
\frac{n_5(t+\Delta t) - n_5(t)}{\Delta t} = +2m\eta(t) + \frac{eB}{2\pi^2}eE(t) \tag{A12}
$$

By taking limit $\Delta t \to 0$, the anomaly relaion is obtained. The anomaly relation for massless fermion can be proved in the same way.

---

[1] H. Aoi and K. Suzuki, Chirality imbalance and fermion pair production under the strong electromagnetic field, in *Proceedings of the 8th International Conference on Quarks and Nuclear Physics (QNP2018)*, https://journals.jps.jp/doi/pdf/10.7566/JPSCP.26.031025.

[2] H. Aoi and K. Suzuki, Phys. Rev. D **103**, 036002 (2021).

[3] S. L. Adler, Phys. Rev. **177**, 2426 (1969).

[4] J. S. Bell and R. Jackiw, Il Nuovo Cimento A (1965-1970) **60**, 47 (1969).

[5] Z. Qian, R. Su, and P. K. Yu, Zeitschrift für Physik C Particles and Fields **63**, 651 (1994).

[6] A. Vilenkin, Phys. Rev. D **22**, 3080 (1980).

[7] K. Fukushima, D. E. Kharzeev, and H. J. Warringa, Phys. Rev. D **78**, 074033 (2008).

[8] D. E. Kharzeev, L. D. McLerran, and H. J. Warringa, Nuclear Physics A **803**, 227 (2008).

[9] D. T. Son and P. Surówka, Phys. Rev. Lett. **103**, 191601 (2009).

[10] D. E. Kharzeev, Progress in Particle and Nuclear Physics **75**, 133 (2014).

[11] D. Kharzeev, J. Liao, S. Voloshin, and G. Wang, Progress in Particle and Nuclear Physics **88**, 1 (2016).

[12] K. Landsteiner, Acta Phys. Pol. B **47**, 2617 (2016).

[13] V. Roy and S. Pu, Phys. Rev. C **92**, 064902 (2015).

[14] H. Li, X.-l. Sheng, and Q. Wang, Phys. Rev. C **94**, 044903 (2016).

[15] J. Zhao and F. Wang, Progress in Particle and Nuclear Physics **107**, 200 (2019).

[16] S. A. Voloshin, Phys. Rev. Lett. **105**, 172301 (2010).

[17] S. Shi, H. Zhang, D. Hou, and J. Liao, Phys. Rev. Lett. **125**, 242301 (2020).

[18] X.-L. Zhao, G.-L. Ma, and Y.-G. Ma, Phys. Rev. C **99**, 034903 (2019).

[19] Y. Feng, Y. Lin, J. Zhao, and F. Wang, Physics Letters B **820**, 136549 (2021).

[20] B. Q. Lv, H. M. Weng, B. B. Fu, X. P. Wang, H. Miao, J. Ma, P. Richard, X. C. Huang, L. X. Zhao, G. F. Chen, Z. Fang, X. Dai, T. Qian, and H. Ding, Phys. Rev. X **5**, 031013 (2015).

[21] Q. Li, D. E. Kharzeev, C. Zhang, Y. Huang, I. Pletikosić, A. V. Fedorov, R. D. Zhong, J. A. Schneeloch, G. D. Gu, and T. Valla, Nature Physics **12**, 550 (2016).

[22] Z. Zheng, Z. Lin, D.-W. Zhang, S.-L. Zhu, and Z. D. Wang, Phys. Rev. Research **1**, 033102 (2019).

[23] J. Xiong, S. K. Kushwaha, T. Liang, J. W. Krizan, M. Hirschberger, W. Wang, R. J. Cava, and N. P. Ong, Science **350**, 413 (2015),

https://www.science.org/doi/pdf/10.1126/science.aac6089.

[24] D. E. Kharzeev, Annals of Physics **325**, 205 (2010), january 2010 Special Issue.

[25] N. Müller, S. Schlichting, and S. Sharma, Phys. Rev. Lett. **117**, 142301 (2016).

[26] M. A. Metlitski and A. R. Zhitnitsky, Phys. Rev. D **72**, 045011 (2005).

[27] G. M. Newman and D. T. Son, Phys. Rev. D **73**, 045006 (2006).

[28] D. E. Kharzeev and H.-U. Yee, Phys. Rev. D **83**, 085007 (2011).

[29] Y. Burnier, D. E. Kharzeev, J. Liao, and H.-U. Yee, Phys. Rev. Lett. **107**, 052303 (2011).

[30] L. Adamczyk, J. K. Adkins, G. Agakishiev, M. M. Aggarwal, Z. Ahammed, I. Alekseev, J. Alford, A. Aparin, D. Arkhipkin, E. C. Aschenauer, G. S. Averichev, A. Banerjee, R. Bellwied, A. Bhasin, A. K. Bhati, P. Bhattarai, J. Bielcik, J. Bielcikova, L. C. Bland, I. G. Bordyuzhin, J. Bouchet, A. V. Brandin, I. Bunzarov, T. P. Burton, J. Butterworth, H. Caines, M. Calderón de la Barca Sánchez, J. M. Campbell, D. Cebra, M. C. Cervantes, I. Chakaberia, P. Chaloupka, Z. Chang, S. Chattopadhyay, J. H. Chen, X. Chen, J. Cheng, M. Cherney, W. Christie, G. Contin, H. J. Crawford, S. Das, L. C. De Silva, R. R. Debbe, T. G. Dedovich, J. Deng, A. A. Derevschikov, B. di Ruzza, L. Didenko, C. Dilks, X. Dong, J. L. Drachenberg, J. E. Draper, C. M. Du, L. E. Dunkelberger, J. C. Dunlop, L. G. Efimov, J. Engelage, G. Eppley, R. Esha, O. Evdokimov, O. Eyser, R. Fatemi, S. Fazio, P. Federic, J. Fedorisin, Z. Feng, P. Filip, Y. Fisyak, C. E. Flores, L. Fulek, C. A. Gagliardi, D. Garand, F. Geurts, A. Gibson, M. Girard, L. Greiner, D. Grosnick, D. S. Gunarathne, Y. Guo, S. Gupta, A. Gupta, W. Guryn, A. Hamad, A. Hamed, R. Haque, J. W. Harris, L. He, S. Heppelmann, S. Heppelmann, A. Hirsch, G. W. Hoffmann, D. J. Hofman, S. Horvat, H. Z. Huang, B. Huang, X. Huang, P. Huck, T. J. Humanic, G. Igo, W. W. Jacobs, H. Jang, K. Jiang, E. G. Judd, S. Kabana, D. Kalinkin, K. Kang, K. Kauder, H. W. Ke, D. Keane, A. Kechechyan, Z. H. Khan, D. P. Kikola, I. Kisel, A. Kisiel, D. D. Koetke, T. Kollegger, L. K. Kosarzewski, L. Kotchenda, A. F. Kraishan, P. Kravtsov, K. Krueger, I. Kulakov, L. Kumar, R. A. Kycia, M. A. C. Lamont, J. M. Landgraf, K. D. Landry, J. Lauret, A. Lebedev, R. Lednicky, J. H. Lee, W. Li, Y. Li, C. Li, N. Li, Z. M. Li, X. Li, X. Li, M. A. Lisa, F. Liu, T. Ljubicic, W. J. Llope, M. Lomnitz, R. S. Longacre, X. Luo, L. Ma, R. Ma, Y. G. Ma, G. L. Ma, N. Magdy, R. Majka, A. Manion, S. Margetis, C. Markert, H. Masui, H. S. Matis, D. McDonald, K. Meehan, N. G. Minaev, S. Mioduszewski, B. Mohanty, M. M. Mondal, D. A. Morozov, M. K. Mustafa, B. K. Nandi, M. Nasim, T. K. Nayak, G. Nigmatkulov, L. V. Nogach, S. Y. Noh, J. Novak, S. B. Nurushev, G. Odyniec, A. Ogawa, K. Oh, V. Okorokov, D. L. Olvitt, B. S. Page, R. Pak, Y. X. Pan, Y. Pandit, Y. Panebratsev, B. Pawlik, H. Pei, C. Perkins, A. Peterson, P. Pile, M. Planinic, J. Pluta, N. Poljak, K. Poniatowska, J. Porter, M. Posik, A. M. Poskanzer, N. K. Pruthi,

J. Putschke, H. Qiu, A. Quintero, S. Ramachandran, S. Raniwala, R. Raniwala, R. L. Ray, H. G. Ritter, J. B. Roberts, O. V. Rogachevskiy, J. L. Romero, A. Roy, L. Ruan, J. Rusnak, O. Rusnakova, N. R. Sahoo, P. K. Sahu, I. Sakrejda, S. Salur, J. Sandweiss, A. Sarkar, J. Schambach, R. P. Scharenberg, A. M. Schmah, W. B. Schmidke, N. Schmitz, J. Seger, P. Seyboth, N. Shah, E. Shahaliev, P. V. Shanmuganathan, M. Shao, B. Sharma, M. K. Sharma, W. Q. Shen, S. S. Shi, Q. Y. Shou, E. P. Sichtermann, R. Sikora, M. Simko, M. J. Skoby, D. Smirnov, N. Smirnov, L. Song, P. Sorensen, H. M. Spinka, B. Srivastava, T. D. S. Stanislaus, M. Stepanov, R. Stock, M. Strikhanov, B. Stringfellow, M. Sumbera, B. J. Summa, X. Sun, X. M. Sun, Z. Sun, Y. Sun, B. Surrow, D. N. Svirida, M. A. Szelezniak, Z. Tang, A. H. Tang, T. Tarnowsky, A. N. Tawfik, J. H. Thomas, A. R. Timmins, D. Tlusty, M. Tokarev, S. Trentalange, R. E. Tribble, P. Tribedy, S. K. Tripathy, B. A. Trzeciak, O. D. Tsai, T. Ullrich, D. G. Underwood, I. Upsal, G. Van Buren, G. van Nieuwenhuizen, M. Vandenbroucke, R. Varma, A. N. Vasiliev, R. Vertesi, F. Videbaek, Y. P. Viyogi, S. Vokal, S. A. Voloshin, A. Vossen, F. Wang, Y. Wang, H. Wang, J. S. Wang, Y. Wang, G. Wang, G. Webb, J. C. Webb, L. Wen, G. D. Westfall, H. Wieman, S. W. Wissink, R. Witt, Y. F. Wu, Z. Xiao, W. Xie, K. Xin, Y. F. Xu, N. Xu, Z. Xu, Q. H. Xu, H. Xu, Y. Yang, Y. Yang, C. Yang, S. Yang, Q. Yang, Z. Ye, P. Yepes, L. Yi, K. Yip, I.-K. Yoo, N. Yu, H. Zbroszczyk, W. Zha, X. P. Zhang, J. B. Zhang, J. Zhang, Z. Zhang, S. Zhang, Y. Zhang, J. L. Zhang, F. Zhao, J. Zhao, C. Zhong, L. Zhou, X. Zhu, Y. Zoulkarneeva, and M. Zyzak (STAR Collaboration), Phys. Rev. Lett. **114**, 252302 (2015).

[31] M. M. Vazifeh and M. Franz, Phys. Rev. Lett. **111**, 027201 (2013).

[32] N. Yamamoto, Phys. Rev. D **92**, 085011 (2015).

[33] V. A. Rubakov, On chiral magnetic effect and holography (2010), arXiv:1005.1888 [hep-ph].

[34] A. Rebhan, A. Schmitt, and S. A. Stricker, Journal of High Energy Physics **2010**, 26 (2010).

[35] M. A. Zubkov, Phys. Rev. D **93**, 105036 (2016).

[36] B. Feng, D.-f. Hou, H. Liu, H.-c. Ren, P.-p. Wu, and Y. Wu, Phys. Rev. D **95**, 114023 (2017).

[37] D.-f. Hou, H. Liu, and H.-c. Ren, Journal of High Energy Physics **2011**, 46 (2011).

[38] P. Copinger, K. Fukushima, and S. Pu, Phys. Rev. Lett. **121**, 261602 (2018).

[39] S. Lin and L. Yang, Phys. Rev. D **98**, 114022 (2018).

[40] O. Klein, Zeitschrift für Physik **53**, 157 (1929).

[41] F. Sauter, Zeitschrift für Physik **69**, 742 (1931).

[42] W. Heisenberg and H. Euler, Zeitschrift für Physik **98**, 714 (1936).

[43] J. Schwinger, Phys. Rev. **82**, 664 (1951).

[44] K. Tuchin, Advances in High Energy Physics **2013**, 490495 (2013).

[45] P. Solinas, A. Amoretti, and F. Giazotto, Phys. Rev. Lett. **126**, 117001 (2021).

[46] A. G. Green and S. L. Sondhi, Phys. Rev. Lett. **95**, 267001 (2005).

[47] T. Oka, R. Arita, and H. Aoki, Phys. Rev. Lett. **91**, 066406 (2003).

[48] T. Oka, Phys. Rev. B **86**, 075148 (2012).

[49] F. m. c. Fillion-Gourdeau and S. MacLean, Phys. Rev. B **92**, 035401 (2015).

[50] B. S. Xie, Z. L. Li, and S. Tang, Matter and Radiation at Extremes **2**, 225 (2017).

[51] N. Tanji, Annals of Physics **324**, 1691 (2009).

[52] P. Copinger and S. Pu, International Journal of Modern Physics A **35**, 203005 (2020), https://doi.org/10.1142/S0217751X2030015X.

[53] H. J. Warringa, Phys. Rev. D **86**, 085029 (2012).

[54] V. Domcke, Y. Ema, and K. Mukaida, Journal of High Energy Physics **2020**, 55 (2020).

[55] P. W. Anderson, Phys. Rev. **112**, 1900 (1958).

[56] S. Tsuchiya, D. Yamamoto, R. Yoshii, and M. Nitta, Phys. Rev. B **98**, 094503 (2018).

[57] N. Tsuji and H. Aoki, Phys. Rev. B **92**, 064508 (2015).

[58] R. Matsunaga, N. Tsuji, H. Fujita, A. Sugioka, K. Makise, Y. Uzawa, H. Terai, Z. Wang, H. Aoki, and R. Shimano, Science **345**, 1145 (2014), https://science.sciencemag.org/content/345/6201/1145.full.pdf.

[59] F. Gelis and N. Tanji, Progress in Particle and Nuclear Physics **87**, 1 (2016).

[60] H. Taya, H. Fujii, and K. Itakura, Phys. Rev. D **90**, 014039 (2014).